

RESEARCH

Open Access



Diffuse traumatic brain injury induced stimulator of interferons (STING) signaling in microglia drives cortical neuroinflammation, neuronal dysfunction, and impaired cognition

Jonathan M. Packer¹, Samantha G. Giammo¹, Lynde M. Wangler¹, Amara C. Davis¹, Chelsea E. Bray¹ and Jonathan P. Godbout^{1,2,3*}

Abstract

Neuropsychiatric complications including depression and cognitive impairment develop, persist, and worsen in the years after traumatic brain injury (TBI), negatively affecting life and lifespan. Inflammatory responses mediated by microglia are associated with the transition from acute to chronic neuroinflammation after TBI. Moreover, type I interferon (IFN-I) signaling is a key mediator of inflammation during this transition. Thus, the purpose of this study was to determine the degree to which a microglia-specific knockout of the stimulator of interferons (STING) influenced TBI-induced neuroinflammation, neuronal dysfunction, and cognitive impairment. Here, microglial inducible STING knockout (CX₃CR1Cre/ERT2 x STING^{fl/fl}) mice were created and validated (mSTING^{-/-}). Diffuse brain injury (midline fluid percussion) in male and female mice increased STING expression in microglia, promoted microglial morphological restructuring, and induced robust cortical inflammation and pathology 7 days post injury (dpi). These TBI-associated responses were attenuated in mSTING^{-/-} mice. Increased cortical astrogliosis and rod-shaped microglia induced by TBI were independent of mSTING^{-/-}. 7 dpi, TBI induced 237 differentially expressed genes (DEG) in the cortex of functionally wildtype (STING^{fl/fl}) associated with STING, NF-κB, and Interferon Alpha signaling and 85% were attenuated by mSTING^{-/-}. Components of neuronal injury including reduced NeuN expression, increased cortical lipofuscin, and increased neurofilament light chain in plasma were increased by TBI and dependent on mSTING. TBI-associated cognitive tasks (novel object recognition/location, NOR/NOL) at 7 dpi were dependent on mSTING. Notably, the TBI-induced cognitive deficits in NOR/NOL and increased cortical inflammation 7 dpi were unaffected in global interferon-α/β receptor 1 knockout (IFNAR1) mice. In the final study, the RNA profile of neurons after TBI in STING^{fl/fl} and mSTING^{-/-} mice was assessed 7 dpi by single nucleus RNA-sequencing. There was a TBI-dependent suppression of cortical neuronal homeostasis with reductions in CREB signaling, synaptogenesis, and oxytocin signaling and increases in cilium assembly and PTEN signaling. Overall, mSTING^{-/-} prevented 50% of TBI-induced DEGs in cortical neurons. Collectively, ablation of STING in microglia attenuates TBI-induced interferon responses, cortical inflammation, neuronal dysfunction, neuronal pathology, and cognitive impairment.

Keywords Microglia, TBI, Inflammation, Cognitive Dysfunction, Stimulator of Interferon Genes, And Type I Interferons

*Correspondence:

Jonathan P. Godbout

Jonathan.Godbout@osumc.edu

Full list of author information is available at the end of the article



© The Author(s) 2025. **Open Access** This article is licensed under a Creative Commons Attribution-NonCommercial-NoDerivatives 4.0 International License, which permits any non-commercial use, sharing, distribution and reproduction in any medium or format, as long as you give appropriate credit to the original author(s) and the source, provide a link to the Creative Commons licence, and indicate if you modified the licensed material. You do not have permission under this licence to share adapted material derived from this article or parts of it. The images or other third party material in this article are included in the article's Creative Commons licence, unless indicated otherwise in a credit line to the material. If material is not included in the article's Creative Commons licence and your intended use is not permitted by statutory regulation or exceeds the permitted use, you will need to obtain permission directly from the copyright holder. To view a copy of this licence, visit <http://creativecommons.org/licenses/by-nc-nd/4.0/>.

Introduction

Neuropsychiatric complications including depression and cognitive decline develop and even worsen in the years following traumatic brain injury (TBI). These complications negatively affect quality of life and lifespan. On average, there are 2.4 million brain injuries per year in the United States alone [1]. TBI also increases the risk of dementia and progressive neurodegeneration [2]. Microglia, the innate immune cell of the central nervous system (CNS), are involved in chronic inflammation and progressive neurodegeneration after TBI [3–5]. For example, microglial activation is detected acutely, and evidence of this activation can persist months to years post-TBI in humans [6–9]. Microglia and corresponding inflammation after TBI affects brain regions responsible for cognition and executive function, impairing information processing, memory, and executive function [3–5]. Thus, understanding the specific pathways induced in microglia after TBI that promote chronic inflammatory processes is a biologically relevant area of focus.

Myriad reports indicate that TBI-induced chronic neuroinflammation and cognitive dysfunction in rodents are dependent on microglial responses [4, 10–14]. We and others have reported that there is a pronounced shift in microglia RNA profiles from pro-inflammatory and NF- κ B mediated genes towards a type 1 interferon (IFN-I) response at a subacute time point after TBI (7 days post injury, dpi) [11, 12, 15]. For instance, single-cell RNA sequencing (scRNA-seq) identified trauma-associated microglia 7 dpi in the cortex with a transcriptional signature that was enriched for IFN-I responses (*Ifitm3*, *Stat1*, *Irf7*, *Ifi2712a*) and inflammasome activation [11]. Cortical RNA gene expression also showed the amplification of IFN-I responses 7 dpi [11, 12]. Depletion of microglia prior to TBI using a CSF1R antagonist (PLX5622) attenuated neuroinflammation and ablated the IFN-I response after diffuse TBI. These reductions corresponded with improved cortical dendritic complexity, neuronal physiology, and cognition in novel object location and recognition tasks [11]. Notably, the subacute period after TBI (7 dpi) involved enhanced interferon responses and was worse with age. For instance, diffuse or penetrating TBI in aged mice amplified IFN-I genes (*Ifn- β* , *Irf7*, *Ifi204*, and *Isg15*) [16, 17]. In addition, there was amplified IFN-I responses and enhanced gliosis and neuroinflammation in the cortex of aged mice after diffuse TBI [16]. Overall, IFN-I responses are dominant in the brain during the subacute period (7 dpi) after diffuse TBI.

The normal dynamics between microglia and neurons are disrupted by TBI [18]. For example, microglial activation after diffuse and penetrating TBI influences neuronal homeostasis with increased neuron loss, neuronal synapse degradation [19], reduced dendritic complexity

[10, 11], and post-synaptic density loss [20]. Moreover, microglia depletion with the CSF1R antagonist PLX5622, improved neuronal physiology [10, 11], neuronal dendritic restructuring [10, 11], and cognitive deficits following TBI [11–13, 21, 22]. Furthermore, microglial depletion and repopulation following TBI improved dendritic complexity, compound action potential recordings, and novel object location/recognition [10, 13]. Taken together, microglial responses in the subacute and chronic phases following TBI disrupt the homeostasis of neurons.

The shift in the inflammatory profile at the subacute period after TBI is pertinent and involves the stimulator of IFN genes (STING). STING is a stress-responsive endoplasmic reticulum protein. In the context of viral infection or injury, tissue damage increases cytosolic double-stranded DNA (dsDNA) and mitochondrial DNA (mtDNA) that are sensed by the cGAS-STING pathway [23, 24]. STING promotes IFN-I responses that enhance transcription factors IRF3, and NF- κ B [25, 26] leading to a diverse array of IFN-I and NF- κ B-mediated signaling [24]. Type-1 interferons (IFN- α/β) act on the interferon- α/β receptor 1 (IFNAR1) that is expressed by all cell types within the brain. Furthermore, a recent study of penetrating TBI using controlled cortical impact (CCI) showed that mSTING^{-/-} reduced the acute inflammatory response, lesion volume, and improved motor recovery 72 h post injury [27]. Sub-acutely (7 dpi) after diffuse TBI, the microglial RNA profile (by snRNA-seq) indicated a STING-dependent production of IFN-I (*cGas*, *Tbk1*, *Sting1*). In addition, genes associated with the IFNAR1 (*Ifnar2*, *Stat1*) and interferon stimulated genes (ISGs) (*Mx1*, *Mx2*, *Oasl2*) were also increased in microglia 7 dpi [22]. Consistent with this study, diffuse TBI (lateral fluid percussion injury (FPI)) increased the IFN response in both microglia and astrocytes 7 dpi [15]. In another study, diffuse TBI (midline FPI)-induced STING expression, microglial morphological restructuring, inflammatory, and IFN-related gene expression in the cortex (*Tnf*, *Cd68*, *Ccl2*, *Irf7*, *Sting*) that was attenuated in global STING^{-/-} mice and by a STING antagonist (chloroquine) [22]. Global reductions of STING signaling reduces inflammation, cognitive deficits, and neuronal dysfunction following TBI [22, 28]. Moreover, TBI-associated cognitive deficits (NOR/NOL) at both 7 and 30 dpi were STING dependent [22] and RNA evidence of microglial priming in the cortex 30 dpi was ablated by global STING knockout [22]. Taken together, STING and IFN-I signaling are critical mediators of inflammation, neuronal dysfunction, and cognitive deficits after TBI.

The purpose of this study was to determine the degree to which a microglia-specific knockout of STING influenced neuroinflammation, neuronal dysfunction, and

cognitive impairment induced by diffuse TBI (midline fluid percussion injury, mFPI). This model of diffuse traumatic brain injury was selected because it induces reproducible acute and chronic deficits without overt tissue cavitation [29], neuronal death [12], or chronic infiltration of peripheral immune cells [12, 29]. We show novel data that the selective ablation of STING in microglia attenuates TBI-induced interferon responses, cortical inflammation, neuronal pathology and dysfunction, and cognitive impairment.

Materials and methods

Mice

To generate inducible $CX_3CR1-STING^{-/-}$ mice, $CX_3CR1Cre/ERT2$ (Jax#:020940) and $STING^{fl/fl}$ (Jax#:035692) mice were purchased from The Jackson Laboratory and bred in-house. $CX_3CR1CreERT2$ was selected to induce a knockout of STING in microglia because it is a well-characterized microglia-Cre line with moderately high specificity, low leakiness, and high efficacy of recombination [30, 31]. In addition, mice were used 4 weeks after recombination with tamoxifen to ensure the turnover of peripheral myeloid cells [31], which have a shorter lifespan and higher turnover rate [32, 33]. We acknowledge that other Cre-lines are potentially more specific for microglia, but they have lower efficacy of recombination and higher levels of leakiness into non-microglial cell types [30]. Heterozygous offspring were then backcrossed to generate Cre-ERT2 positive ($CX_3CR1Cre/ERT2-STING^{fl/fl}$) and Cre-negative ($STING^{fl/fl}$) control mice. For genotyping, ear punches biopsies were taken following weaning (21d), and samples were genotyped by TransNetYX (Cordoba, TN).

To induce recombination, Cre-ERT2 positive ($CX_3CR1Cre/ERT2-STING^{fl/fl}$) and Cre-negative control mice ($STING^{fl/fl}$) were administered 1.5 mg of tamoxifen in 150 μ l of corn oil intraperitoneally (i.p.) daily for five days. Mice were allowed 30 days to reconstitute prior to experimental use. The result was a knockout of STING in microglia (Cre-ERT2 positive, $CX_3CR1-STING^{-/-}$ or $mSTING^{-/-}$) or a functional STING wild type (Cre-ERT2-negative, $STING^{fl/fl}$.) Notably, Cre-negative and Cre-positive were used in the experimental design to reduce potential concern with the effects of repeated administrations of tamoxifen compared to mice that receive saline, where repeated tamoxifen injections alone may effect behavioral analyses [34]. In addition, primarily heterozygous Cre-ERT2 mice were used in these experiments (98% of the mice), but there were limited exceptions where sex-matched cage mates were unavailable and homozygous Cre-ERT2 mice were used (2% of the mice). For the global knockout $IFNAR1^{-/-}$ mice,

homozygous male and female $IFNAR1^{-/-}$ mice were purchased from the Jackson Laboratory and bred in-house.

All mice were group housed under a 12/12 light–dark cycle with ad libitum access to food and water. Mice were randomly assigned to groups with mixed treatment and injury groups in each cage. Male and female mice were used in all experiments unless otherwise noted. These experiments, however, were not powered to make sex comparisons. All procedures were performed in accordance with the National Institute of Health Guidelines for the Care and Use of Laboratory Animals, the Public Health Service's Policy on Human Care and Use of Laboratory Animals, and the Guide for the Care and Use of Laboratory Animals and were approved by The Ohio State University Institutional Laboratory Animal Care and Use Committee.

Mouse numbers & exclusion summary

Outlier data values were determined using GraphPad Grubbs' test with an Alpha value of 0.05 selected. Pre-determined cutoffs were used as described [22]. There were 12 $IFNAR1^{+/+}$ and 12 global $IFNAR1$ knockout ($IFNAR1^{-/-}$) mice used in this study. There were no statistical outliers detected in the $IFNAR$ experiments (Fig. 6). There were also 141 $STING^{fl/fl}$ and $CX_3CR1/STING^{-/-}$ mice were used in this study. There were 2 statistical outlier values that were excluded from cognitive analyses (Fig. 1D) and two statistical outlier values were excluded from Fig. 5F–K. There was one statistical outlier value excluded from the NanoString/nCounter analyses (Fig. 3A–I, Fig. 4A–F) and one statistical outlier value excluded from the lipofuscin analysis (Fig. 5C).

Midline fluid percussion injury (mFPI)

Mice were subjected to a midline diffuse TBI using a fluid percussion injury (FPI) apparatus as described previously [12, 22, 35]. Briefly, mice were anesthetized in an isoflurane chamber at 2–3% with a flow rate of 0.8 L/min. After the surgical site was shaved, mice were secured to the stereotactic device (Stoelting Co., Cat# 51,731) and maintained under anesthesia with a mask attachment (Stoelting Co., Cat# 51609 M). The surgical site was prepared with aseptic technique, using alternating applications of iodine and 70% ethanol. Mice received a 3 mm craniectomy between the landmark sutures bregma and λ , and a rigid Luer-loc needle hub was secured over the craniectomy site. Following this procedure, mice were moved to a heated (37 °C) recovery cage and monitored until conscious (upright, responsive, and walking). After recovery, mice were briefly re-anesthetized in an isoflurane chamber at 5% (flow rate 0.8 L/min) for 5 min. The Luer-loc hub was filled with saline, and the hub was attached to the injury device. Once a positive toe-pinch response was

elicited (~30 s), a 10 ms pulse of saline (1.2 atm; 670–720 mV) was imposed on the dura. Immediately after the TBI, the Luer-loc hub was removed, dural integrity was confirmed. Next, wound clips (7 mm) were used to close the incision site and the time to self-right was determined (upright and responsive). Next, mice were moved to a heated cage overnight. In these studies, control mice were naïve and uninjured.

Post-op care

Mice with TBI were monitored for 1 h post-injury and then allowed to recover overnight in a heated recovery cage with accessible food and hydrogel. The next day, mice were returned to their home cages. In these experiments, no analgesics were provided. Mice were weighed and monitored for lethargy (lack of movement) and infection (redness and pus around the incision site) daily throughout the experiments (7 days). Removal criteria included a loss of 20% of baseline bodyweight, sustained lethargy, paralysis, or surgical site infection. In this study, 5 mice were removed based on these criteria.

Immunohistochemistry and analysis

Mice were perfused with phosphate buffered saline (PBS) followed by 4% PFA. Brains were removed, post-fixed, and dehydrated in 30% sucrose. Brains were flash-frozen via isopentane, and then coronal sections (30 μ m) were collected, washed, blocked, (0.1% Triton X, 5% BSA, and 5% NDS) and incubated with primary antibodies for rabbit anti-IBA1 (1:1000, Wako, Cat#019–19741, RRID:AB_839504), goat anti-IBA1 (1:500, Wako, #011–27991, RRID:AB_2935833), goat anti-GFAP (1:500, Abcam Cat#ab53554, RRID:AB_880202), rabbit anti-STING (1:200, Proteintech, #19,851–1-AP, RRID:AB_10665370), or mouse anti-NeuN (1:500, Abcam, Cat#ab104225, RRID:AB_10711153). Next, sections were washed, incubated with an appropriate fluorochrome-conjugated secondary antibody (donkey anti-rabbit, anti-mouse, or anti-goat; AlexaFluor

488/594/647; Invitrogen) then mounted and coverslipped with Fluoromount (Beckman Coulter, Inc., Fullerton, CA). Fluorescent labeling was imaged using an EVOS FL Auto 2 imaging system (Thermo Fisher, Waltham, MA). To determine percent area of IBA1⁺, GFAP⁺, STING⁺, or NeuN⁺ labeling, single channel images were converted to 8-bit TIFF format and constant thresholds were used to quantify positively labeled pixels (ImageJ Software). Rod morphology of IBA1⁺ microglia were quantified based on length-to-width ratios as previously described [12]. Values from 4–6 images per mouse were averaged and used to calculate group averages and variance from each group. To determine the number of Lipofuscin⁺ foci, 10 NeuN⁺ cells were selected at random, and foci were counted. Lipofuscin (autofluorescence) was detected at 455 nm excitation and 583 nm emission [36]. To determine co-labeling of IBA1⁺ and STING⁺ or Lipofuscin⁺ and NeuN⁺ single channel images were converted to 8-bit TIFF format and Just Another Co-localization Plugin (JaCoP) was used to determine the double labeling (Image J Software). For double-labeling, 4–6 images per mouse were taken using a Nikon Ti2 inverted motorized microscope. Images were taken at 10 \times magnification as 13 μ m z stacks. Denoise.ai was used to reduce background and increase image intensity. Images were analyzed by an investigator blinded to treatment groups.

Nanostring and ncounter analysis

NanoString nCounter tissue collection and analysis was performed as previously described [12, 16, 37]. Each experimental group was duplicated in separate experiments, yielding four total experimental groups, with six biological replicates per group. In brief, cortex was collected 7 dpi, flash frozen in liquid nitrogen, and stored –80 °C. RNA was isolated using the TRI-Reagent and isopropanol protocol (Sigma-Aldrich). RNA quality and integrity were confirmed using a BioAnalyzer PicoAssay by Chip (Agilent). Gene expression was quantified using the nCounter NanoString neuroinflammation panel

(See figure on next page.)

Fig. 1 TBI-induced STING expression in microglia was ablated by mSTING^{-/-}. **A** To generate the inducible and microglia specific knockout of STING, C57BL/6-STING^{fl/fl} mice were crossed with CX₃CR1-Cre/ERT2 mice. Mice were backcrossed and genotyped to establish CX₃CR1/STING^{fl/fl} mice (Cre-ERT2⁺) and STING^{fl/fl} (Cre-ERT2^{neg}) lines. Recombination was induced with tamoxifen (10 mg/ml in corn oil, i.p.) four weeks prior to experiments to generate CX₃CR1/STING^{-/-} (mSTING^{-/-}) mice. **B** Male and female functional wild type (STING^{fl/fl}) and mSTING^{-/-} mice were subjected to midline fluid percussion injury or left as uninjured controls. Several parameters were determined 7 dpi including determination of STING (RNA and protein) in microglia. **C** Time to self-right for functional wild type (STING^{fl/fl}) and CX₃CR1/STING^{-/-} (or mSTING^{-/-}) mice immediately following TBI (n = 9–14). **D** *Sting* (*Tmem173*) RNA determined in percoll-enriched microglia collected from the whole brain 7 dpi (n = 4–6). **E** Representative images of STING⁺ labeling (10 \times , 500 μ m) in the cortex 7 dpi. Right panels show enlarged images of positive STING labeling in TBI-STING^{fl/fl} and TBI-mSTING^{-/-} mice. **F** Percent-area of STING⁺ labeling in the cortex 7 dpi (n = 6–8). From the same experiment, **G** Representative images of STING⁺ and IBA1⁺ labeling (n = 6–8). **G** Right panel shows percent of double labeled IBA1⁺ and STING⁺ cells 7 dpi in the cortex. Bars represent the mean \pm SEM, and individual data points are provided. Means with (*) are significantly different from control groups ($p < 0.05$) and means with (†) are significantly different from all other groups ($p < 0.05$)

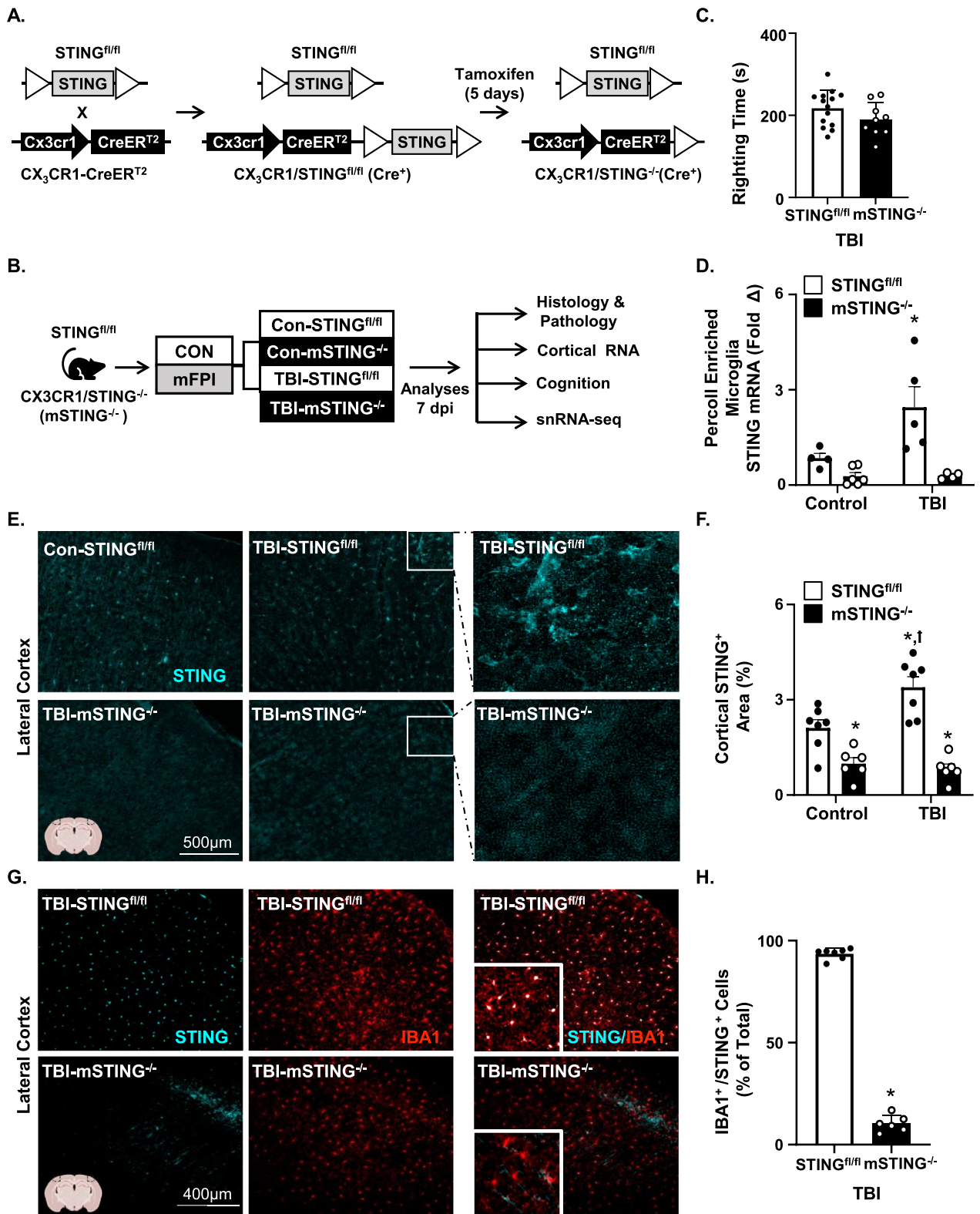


Fig. 1 (See legend on previous page.)

targeting 770 genes (<https://nanosttring.com/>). This was performed by the Genomics Core facility at The Ohio State University. Technical normalization was performed to positive and negative controls. Cortical RNA was normalized to the housekeeping gene *Csnk2a2*. This housekeeping gene was selected based on strong correlation with total counts ($R^2 > 0.8$). Differential gene expression analyses were performed using the DESeq2 package in R Studio. Results were generated based on injury, genotype and sex (e.g., TBI-STING^{fl/fl} vs TBI-mSTING^{-/-}). Statistically significant genes had a threshold set to $p\text{-adj} < 0.05$. Ingenuity Pathway Analysis (IPA, Qiagen) was used to identify canonical pathways associated with the significant genes compared to the respective control (Con-STING^{fl/fl} or Con-mSTING^{-/-}). Results from IPA are represented by z-score. Gene names and fold changes were submitted to compare expression patterns in our dataset to IPA's database. IPA results for canonical pathways ($p < 0.05$; composite z-score > 2) were considered significant. Upstream Regulators were further filtered for activation z-scores (positive or negative) that were associated with either increased or decreased signaling.

Percoll enrichment of microglia

Microglia/myeloid cells (CD11b⁺) were enriched from whole brain homogenates at 7 dpi as described [10, 35, 38]. In brief, brains were manually homogenized using Potter homogenizers, and resulting homogenates were pelleted at 600 g for 6 min. Supernatants were removed and cell pellets were resuspended in 70% isotonic Percoll (GE-Healthcare, Catalog #45-001-747). A discontinuous isotonic Percoll density gradient was layered as follows: 50%, 35%, and 0% (PBS). Samples were pelleted for 20 min at 2000 g, and cells were collected from the interphase between the 70% and 50% Percoll layers. These cells are referred to as enriched microglia/myeloid cells based on previous studies demonstrating that viable cells isolated by Percoll density gradient yields over 90% CD11b⁺ cells [38]. Moreover, there is not significant accumulation of peripheral myeloid cells with mFPI at 7 dpi [11, 39], so these myeloid cells are represented as percoll-enriched microglia.

RNA extraction and qPCR

Percoll-enriched myeloid cells were lysed, stored at -80°C , and total RNA was extracted using the Picopure RNA Isolation Kit (ThermoFisher, KIT0204). RNA was normalized by concentration and reverse-transcribed to cDNA. The Applied Biosystems Taqman Gene Expression assay-on-demand protocol and recommended probes for each gene of interest was used for quantitative real-time PCR. Target genes including *Tmem173* (*Sting*): Mm01158117_m1, *H2-Eb1*: Mm00439221_m1,

Irf7: Mm00516791_g1, *Cd68*: Mm03047343_m1, *Tnf*: Mm00443258_m1, and reference gene *Gapdh*: Mm99999915_g were determined using a QuantStudio 6 (Thermo Fisher) and data were analyzed using the comparative threshold method ($\Delta\Delta\text{Ct}$) with data expressed as fold-change from control.

Novel object recognition (NOR) and location (NOL)

Novel object recognition (NOR) and novel object recognition (NOL) tasks were conducted as previously described [10, 11]. Briefly, these tests involved four 10 min phases each separated by 24 h: habituation (no objects), acclimation (2 objects), recognition (2 objects, with one new object), and location (2 objects, one new location). Discrimination index in the recognition and location trials was determined $[(\text{time}_{\text{novel}} - \text{time}_{\text{familiar}}) / \text{time}_{\text{total}}] \times 100$. Videos were analyzed by an investigator blinded to treatment groups.

Plasma neurofilament analysis

Plasma neurofilament was assessed in duplicate using a Meso Scale Discovery R-PLEX Human Neurofilament L Assay (K1517XR-2) according to the manufacturer's instructions and as described previously [40]. In brief, mice were euthanized, blood was collected and clarified at 6000g for 15 min, and plasma was frozen at -80°C until analysis. Neurofilament light chain (NF-L) was analyzed in plasma samples diluted two-fold. The concentration of neurofilament light chain (NF-L) (pg/ml) was determined using the MESO QuickPlex SQ 120 with reference to a standard curve. The standard curve was established using 8 provided calibrator standards (0–50,000 pg/mL). All samples were within the detection range of the standards.

Nuclei isolation

Nuclei were isolated for single nucleus RNA-sequencing as previously described [22]. In brief, each group ($n=3$) was sacrificed simultaneously, then pooled. Each experimental group was duplicated in separate experiments, yielding four total experimental groups, with six biological replicates per group. Cortices were extracted then placed into 2 mL Dounce homogenizers with 1 mL of homogenization buffer. Cortices were homogenized, filtered using a 40 μM strainer and homogenates were clarified. Samples were resuspended in a PBS buffer with RNase Inhibitors (0.05 U/ μL of Enzymatics RNAase-Inhibitor and Superase-Inhibitor) and re-pelleted. To remove myelin debris, samples were incubated with Myelin Removal Beads II (Miltenyi Biotec, #130-096-731) for 15 min at 4°C . Samples were washed (50% PBS and 50% PBS+1% BSA) and re-pelleted. Supernatant was removed and samples were resuspended in 1 mL of wash

buffer. Two LS columns (Miltenyi Biotec, Cat #130-042-401) were used to filter each of the samples, which were then pelleted and resuspended in 150 μ L of wash buffer. Nuclei were counted with AO/PI (Logos Biosystems, #F23001) on a Luna-FL Cell Counter and fixed with a Nuclei Fixation Kit (Parse Biosciences, #SB1003) per the manufacturer's instructions followed by rapid freezing at -80°C .

Single-nuclei barcoding and sub-library generation

As previously described [22], The Parse Biosciences Whole Transcription Kit was used to barcode and generate eight separate sub-libraries with 12,500 nuclei per sub-library. DNA concentration was measured by Qubit 4 Fluorometer and a Qubit dsDNA HS Assay Kit (Thermo Fisher Scientific, #Q32851). A Bioanalyzer 2100 with a High Sensitivity DNA Assay chip was used to control quality of sub-libraries before samples were sequenced. Based on previous sequencing experiments, RNA was sequenced at a depth of 40,000 reads per nuclei using a NovaSeq S4 at the Advanced Genomics Core at The University of Michigan [22].

Single-nuclei sequencing data processing

Libraries were processed as previously described [22]. In brief, each fastq.gz file was downloaded and aligned to the Genome Reference Consortium Mouse Reference 39 (mm39) using the Parse Biosciences pipeline. Matrices were downloaded and manually filtered in RStudio using Seurat (v4.1.1). Low-quality nuclei and doublets were filtered using Seurat in R. Cell-type identification was done using previously established markers: endothelial cells (*Flt1*), astrocytes (*Slc1a3*), oligodendrocytes (*Mag*), microglia (*Csf1r*), and neurons (*Syt1*). Differential gene expression was performed using the FindMarkers feature of Seurat with non-parametric Wilcoxon rank sum test. Pathway and master regulators analyses were performed with Ingenuity Pathway Analysis (IPA; Qiagen).

Statistical analysis

GraphPad Prism (Version 9; San Diego, CA) was used for analysis of variance (ANOVA) of histological and behavioral data. A Student's t test was used as appropriate to determine differences between groups. Two-way ANOVA was used as appropriate to determine main effects and interactions between factors. Tukey's test for multiple comparisons was used for *post-hoc* analysis when main effects and/or interactions were determined. $p < 0.05$ was considered statistically significant. Statistical analysis for snRNA-sequencing using Seurat are described above. Outlier data values were determined using GraphPad Grubbs' test with an Alpha value of 0.05 selected.

Results

TBI-induced STING expression in microglia was ablated by mSTING^{-/-}

We previously reported that a global STING knockout reduced TBI-associated neuroinflammation (Interferon signaling and microglia activation) and cognitive impairment [22]. Here, we sought to understand the cell specificity of STING signaling in microglia after diffuse TBI. First, a transgenic mouse line with an inducible knockout of STING in microglia was created (STING^{fl/fl} or mSTING^{-/-}, Fig. 1A). Next, STING^{fl/fl} and mSTING^{-/-} mice were subjected to control or TBI (mFPI) and several parameters were evaluated 7 dpi (Fig. 1B). Time to self-right was assessed immediately after TBI. There were no differences between STING^{fl/fl} and mSTING^{-/-} mice in self-righting times following TBI (Fig. 1C). Next, *Sting* mRNA was determined in percoll-enriched microglia collected from the whole brain 7 dpi (Fig. 1D). As expected, there was a main effect of genotype on *Sting* mRNA levels in microglia ($F_{1,15} = 14.2$, $p < 0.005$) where mSTING^{-/-} mice had the lowest expression of STING. Moreover, TBI increased STING mRNA in enriched microglia 7 dpi ($F_{1,15} = 5.0$, $p < 0.05$), which was ablated in mSTING^{-/-} mice (Interaction, $F_{1,15} = 4.8$, $p < 0.05$). Post-hoc analysis confirmed TBI-STING^{fl/fl} mice had the highest expression of *Sting* in microglia compared to all other groups ($p < 0.05$). These mRNA data validate the knockout of *Sting* in microglia.

Next, STING protein was assessed in the cortex 7 dpi (Fig. 1E, F). Parallel to the mRNA data, TBI increased STING protein expression ($F_{1,22} = 4.65$, $p < 0.05$) in the cortex 7 dpi, which was influenced by genotype ($F_{1,22} = 52.10$, $p < 0.0001$) with less STING protein expression in the mSTING^{-/-} mice compared to STING^{fl/fl} mice (Fig. 1E, F). Post-hoc analyses confirmed that TBI-STING^{fl/fl} mice had the highest levels of STING in the cortex ($p < 0.001$). Parallel to these data, STING expression was determined in IBA1⁺ microglia of the cortex 7 dpi. There was robust expression of STING 7 dpi in IBA1⁺ microglia of wild type (STING^{fl/fl}) mice (Fig. 1G, H). Specifically, 94% of IBA1⁺ microglia in the cortex expressed STING after TBI, which was reduced to 10% in the mSTING^{-/-} mice ($p < 0.001$). The reduced STING expression present in control mice was double labeled in 93% of IBA1⁺ cells (data not shown). Notably, there was non-microglia STING expression detected after TBI (Fig. 1F). This increase of STING after TBI, however, was not apparent in cortical astrocytes (GFAP⁺) or neurons (NeuN⁺) (data not shown). These RNA and protein data validate the mSTING^{-/-} model. Overall, STING RNA and protein were increased in microglia 7 dpi, and both were ablated in microglia from the mSTING^{-/-} mice.

TBI-induced microglia reactivity 7 dpi was attenuated by mSTING^{-/-}

Next, cortical gliosis and microglial morphological restructuring was determined 7 dpi in male and female STING^{fl/fl} and mSTING^{-/-} mice. As expected, there was a TBI-dependent increase 7 dpi in the percent area of GFAP⁺ astrocytes ($F_{1,25}=33.56$, $p<0.0001$, Fig. 2A, B) which was independent of mSTING (Fig. 2A, B). There was a main effect of TBI on cortical percent area of IBA1⁺ labeling ($F_{1,25}=55.46$, $p<0.0001$, Fig. 2C, D). This increase of cortical IBA1⁺ after TBI was influenced by mSTING^{-/-} (Interaction, $F_{1,25}=9.30$, $p<0.05$). Post-hoc analyses confirmed that TBI-STING^{fl/fl} mice had the highest IBA1⁺ percent area compared to all groups ($p<0.05$). These increases in IBA1⁺ expression are consistent with “reactive microglia” [41] detected after diffuse TBI [12, 35]. Another aspect of microglial restructuring post-TBI is increased rod-shaped microglia in the cortex [12, 42]. Here, rod-shaped microglia were increased 7 dpi in the medial cortex ($F_{1,24}=11.84$, $p<0.005$, Fig. 2E, F) and this was independent of mSTING. Collectively, the reactive morphological profile of microglia 7 dpi was attenuated by mSTING^{-/-}, but astrogliosis and rod-shaped microglia were unaffected.

TBI-associated cortical inflammation was attenuated by mSTING^{-/-}

In this experiment, cortical inflammation 7 dpi in male and female mice was assessed using NanoString nCounter neuroinflammation panel (770 genes). Differentially expressed genes (DEGs) between groups were determined using DESeq2 in R [43]. The first volcano plot (Fig. 3A) compares TBI-STING^{fl/fl} and Con-STING^{fl/fl} and there were 232 DEGs increased and 5 DEGs decreased after TBI ($p\text{-adj}<0.05$). Figure 3B shows the comparison between TBI-mSTING^{-/-} versus Con-mSTING^{-/-}. There were 76 DEGs increased and no genes decreased by TBI in mSTING^{-/-} mice ($p\text{-adj}<0.05$). Figure 3C shows the comparison between TBI-mSTING^{-/-} mice and TBI-STING^{fl/fl}. There were 2 DEGs increased and 82 DEGs decreased by mSTING^{-/-} ($p\text{-adj}<0.05$). In the comparison between Con-mSTING^{-/-} and Con-mSTING^{fl/fl}, there was only one DEG with increased *Crem* in

mSTING^{fl/fl} mice (Fig. 3D). As stated above, the response to diffuse TBI between male and female mice was similar. To highlight this, the TBI comparison between male and female STING^{fl/fl} mice is shown (Fig. 3E). Only two genes (*Kdm5d*, *Uty*) were differentially expressed after TBI in male and female mice. These DEGs were increased by TBI in males only and are Y-chromosome linked genes [44]. Thus, male and female data were collapsed and analyzed together. Overall, the TBI induced gene expression in the cortex 7 dpi was robustly influenced by mSTING.

These differences are highlighted in Fig. 3F. The Venn diagram represents DEGs that were uniquely increased in TBI-STING^{fl/fl} (173 DEGs), shared between the two groups (64), or unique to TBI-mSTING^{-/-} (12). The pie chart shows the percentage of TBI-associated DEGs (249 total) that were attenuated by mSTING^{-/-} (16%, reduced expression), prevented by mSTING^{-/-} (70%, restoration to control levels), or not prevented by mSTING^{-/-} (14%). The majority of the TBI-induced DEGs were attenuated or prevented by mSTING^{-/-}. Myriad genes increased by TBI were either prevented (*Irf1*, *Ifi30*, *Ilra*, *Irf8*, *Nfkb2*) or attenuated (*Itbg5*, *Itimt3*, *Olfml3*) by mSTING^{-/-} (Fig. 3G, H). Several inflammatory DEGs were increased by TBI and this increase was either attenuated (*C1qb&c*, *Cd68*, *Cxcl10*) or prevented (*Il1a*, *Cd14*, *Irak4*) in the TBI-mSTING^{-/-} mice (Fig. 3G, H). There were also DEGs induced by TBI (*Thr2*, *Thr4*, *Irf7*, *Lcn2*, and *Sox10*) not significantly attenuated or prevented by mSTING^{-/-} (Fig. 3I, J). Overall, the majority (86%) DEGs affected by TBI in the cortex 7 dpi were dependent on STING responses in microglia.

Canonical pathways associated with inflammation and IFN signaling 7 dpi were attenuated by mSTING^{-/-}

Continuing with the NanoString analysis, Ingenuity Pathway Analysis (IPA) was used to determine canonical pathways master regulators, and upstream regulators influenced by TBI or mSTING^{-/-}. Canonical pathways induced by TBI and prevented by mSTING^{-/-} are shown (Fig. 4A). Pathways associated with interferon signaling (cGAS-STING Signaling, Interferon alpha/beta signaling, Interferon Gamma Signaling, Activation of IRF by Cytosolic Pattern Receptors) and neuroinflammation

(See figure on next page.)

Fig. 2 Microglia reactivity 7 dpi was attenuated by mSTING^{-/-}. Male and female functional wild type (STING^{fl/fl}) and CX₃CR1/STING^{-/-} (mSTING^{-/-}) mice were subjected to midline fluid percussion injury or left as uninjured controls. **A** Representative images of GFAP⁺ labeling (10x) in the cortex 7 dpi. Insets show enlarged labeling and right panel shows pseudo-skeletonized GFAP⁺ labeling (white). **B** Percent-area of GFAP⁺ labeling in the cortex 7 dpi (n=6–7). **C** Representative images of IBA1⁺ labeling (10x) in the lateral cortex 7 dpi. Insets show enlarged IBA1⁺ labeling and right panel shows pseudo-skeletonized IBA1⁺ labeling (white). **D** Percent-area of IBA1⁺ labeling in the cortex 7 dpi (n=6–7). **E** Representative images of IBA1⁺ labeling of rod-shaped microglia (10x) in the medial cortex 7 dpi. Insets show enlarged IBA1⁺ labeling and right panel shows pseudo-skeletonized IBA1⁺ labeling (white). **F** Number of IBA1⁺ rod microglia per 10x field in the medial cortex 7 dpi (n=6–7). Means with (*) are significantly different from control groups ($p<0.05$) and means with (^) are significantly different from TBI-STING^{fl/fl} mice ($p<0.05$)

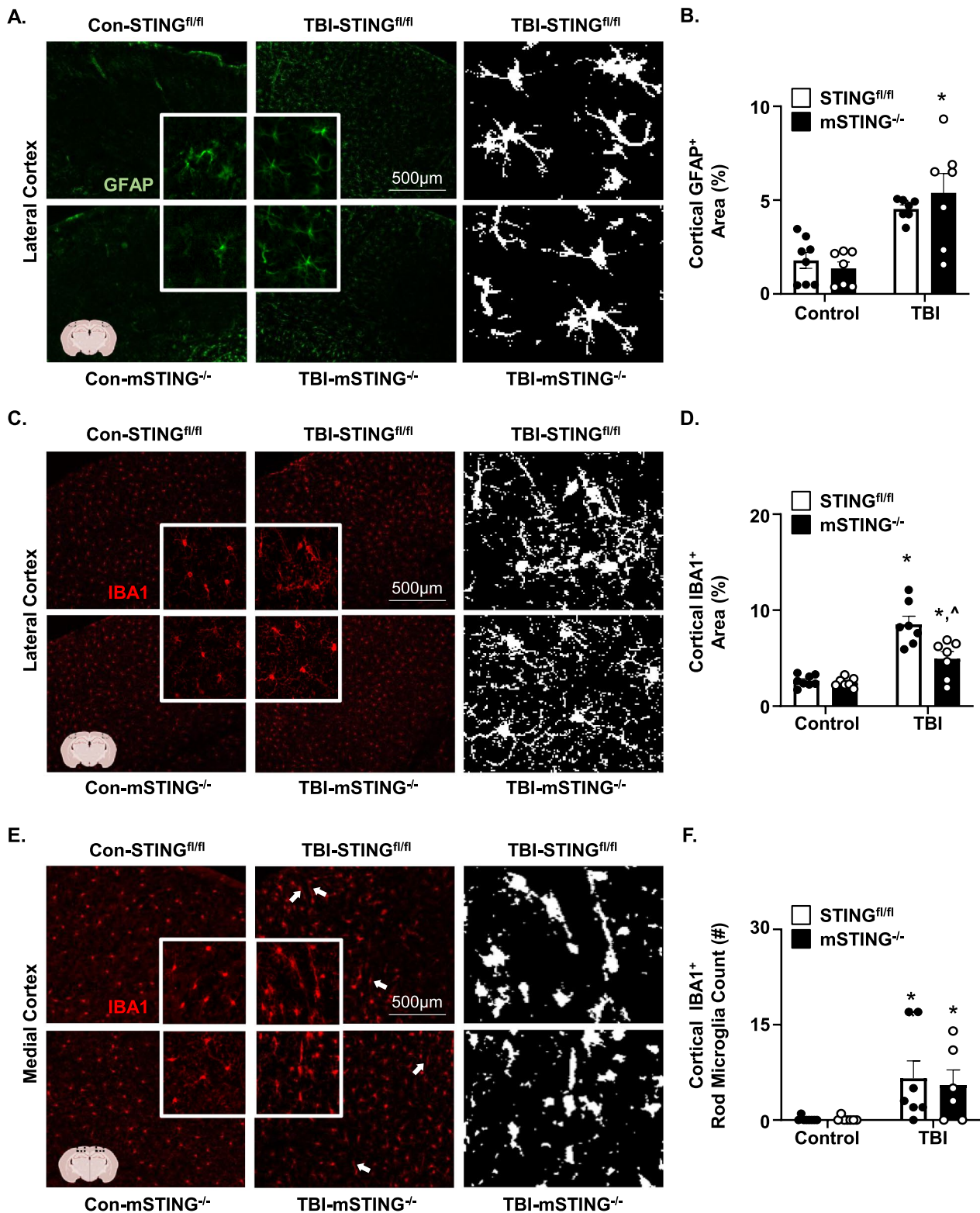


Fig. 2 (See legend on previous page.)

(Phagosome Formation, S100 Family Signaling, Pyroptosis Signaling, Macrophage Classical Activation, NF- κ B Signaling, and iNOS Signaling) were increased in TBI-STING^{fl/fl} mice (p -adj < 0.05). Moreover, these pathways increased by TBI were prevented by mSTING^{-/-} (p -adj < 0.05). Canonical pathways induced by TBI and unaffected mSTING^{-/-} are also shown (Fig. 4B). These mSTING independent pathways included Neutrophil Degranulation, Complement System, Autophagy, and TREM-1 signaling.

Top master regulators induced by TBI and prevented by mSTING^{-/-} are shown (Fig. 4C, D). Master regulators associated with interferon signaling (STAT1, MYD88, IFNG) were increased by TBI while regulators associated with neuronal health (GLB1, NEU3, PTGER4, IRGM1) were decreased. Master regulators prevented by mSTING^{-/-} include pathways associated with IFN-1 (IFNG), neuroinflammation (C5AR1, TREM2, CCR2, IL1B) and neuronal health (LCP1, PTGER4). Next, upstream regulators induced by TBI and prevented by mSTING^{-/-} are shown (Fig. 4E, F). Upstream regulators induced by TBI and prevented by mSTING^{-/-} included pathways associated with phagocytosis (NPC1) and neuroinflammation (IL1B). Taken together, TBI induced myriad inflammatory and interferon-mediated genes that were dependent on STING in microglia.

Neuronal injury and cognitive deficits 7 dpi were mSTING dependent

Our data show that mSTING was important for inflammation after diffuse TBI. Moreover, our previous single cell and single nuclei RNA-seq studies show reduced homeostasis of cortical neurons 7 dpi was dependent on microglia [11, 22]. Based on these data, neuronal health/injury was assessed 7 dpi. First, NeuN⁺ signaling [45] and lipid debris (i.e., lipofuscin) in the cortex were assessed 7 dpi [36, 46]. For NeuN⁺ labeling in the cortex 7 dpi, percent area of NeuN⁺ was influenced by TBI and mSTING^{-/-} (Interaction, $F_{1,24} = 9.68$, $p < 0.005$, Fig. 5A, B). Post hoc analyses indicates that TBI-STING^{fl/fl} mice had the lowest NeuN⁺ expression ($p < 0.05$, Fig. 5B). Lipofuscin accumulation in the brain with age, disease,

or brain injury may also represent reduced homeostasis of neurons and glia [46–48]. There was auto-fluorescent lipid debris visible in the cortex 7 dpi, especially within NeuN⁺ cells (Fig. 5C). Quantification indicates that there tended to be increased auto-fluorescent lipid debris in cortical neurons (NeuN⁺) 7 dpi ($F_{1,19} = 3.19$, $p = 0.08$, Fig. 5D) that tended to be reduced by genotype ($F_{1,19} = 3.93$, $p = 0.06$, Fig. 5D). Thus, there was reduced NeuN⁺ signaling and increased lipofuscin in cortical neurons 7 dpi that was attenuated by mSTING^{-/-}.

Next, neurofilament light chain (NF-L), a relevant biomarker of neural injury after TBI [48], was determined in the plasma of mice [40]. TBI increased NF-L protein (pg/ml) levels ($F_{1,23} = 28.37$, $p < 0.0001$, Fig. 5E), and this increase was influenced by mSTING^{-/-} (Interaction, $F_{1,23} = 9.99$, $p < 0.005$). Post-hoc analyses confirmed TBI-STING^{fl/fl} mice had the highest NF-L (~3,000 pg/ml) protein levels in the plasma ($p < 0.005$). We interpret these results to indicate that TBI increased neuronal injury in the cortex 7 dpi that was dependent on STING in microglia.

In a similar study, control and mSTING^{-/-} mice were subjected to control or TBI (mFPI), and cortical and hippocampal mediated cognition was assessed 7 dpi using NOR/NOL (Fig. 5F–K). There were no differences in total time exploring the objects between groups (Fig. 5F). Figure 5G, H shows TBI-induced reductions in exploration of the novel object 6 dpi (TBI, $F_{1,39} = 24.53$, $p < 0.0001$). Time spent interacting with the novel object was influenced by TBI and mSTING^{-/-} (Interaction, $F_{1,39} = 12.01$, $p < 0.005$, Fig. 5G, H). Post-hoc analyses confirmed that TBI-STING^{fl/fl} mice spent the least amount of time with the novel object ($p < 0.0001$, Fig. 5G, H). These effects and interactions were mirrored in the NOL task at 7 dpi (Fig. 5I–K). Time spent interacting with the novel object was influenced by TBI and mSTING^{-/-} (Interaction, $F_{1,43} = 10.81$, $p < 0.005$, Fig. 5J, K). Post-hoc analyses confirmed that TBI-STING^{fl/fl} mice spent the least amount of time with the novel object ($p < 0.05$, Fig. 5J, K). Overall, microglial STING signaling was critical for neuronal dysfunction and cognitive impairment following TBI.

(See figure on next page.)

Fig. 3 TBI-associated cortical inflammation was attenuated by mSTING^{-/-}. **A** Male and female functional wild type (STING^{fl/fl}) and CX₃CR1/STING^{-/-} (mSTING^{-/-}) mice were subjected to midline fluid percussion injury or left as uninjured controls. Cortices were collected 7 dpi and mRNA expression was determined using NanoString nCounter analyses (n=6). **A** Volcano plot of DEGs in the cortex of TBI-STING^{fl/fl} versus Con-STING^{fl/fl} mice. **B** Volcano plot of DEGs in the cortex of TBI-mSTING^{-/-} versus Con-mSTING^{-/-} mice. **C** Volcano plot of DEGs in the cortex of TBI-mSTING^{-/-} versus TBI-STING^{fl/fl} mice. Red dots represent genes significantly increased with $|\log_2\text{FoldChange}| > 0$ and p -adj < 0.05. Blue dots represent genes significantly decreased with $|\log_2\text{FoldChange}| > 0$ and p -adj < 0.05. Triangles represent the highest DEGs within any volcano plot. **D** Volcano plot of DEGs in the cortex of Con-STING^{-/-} versus Con-STING^{fl/fl} mice. **E** Volcano plot of DEGs in the cortex of male TBI-STING^{fl/fl} versus female TBI-STING^{fl/fl} mice. **F** Percent of genes significantly affected by TBI (TBI-STING^{fl/fl} vs Con-STING^{fl/fl}) that were attenuated, prevented or not prevented in mSTING^{-/-} mice. DEGs that were **(G)** attenuated, **(H)** prevented, **(I)** exacerbated, or **(J)** not prevented are shown in respective heat maps **(F–I)**.

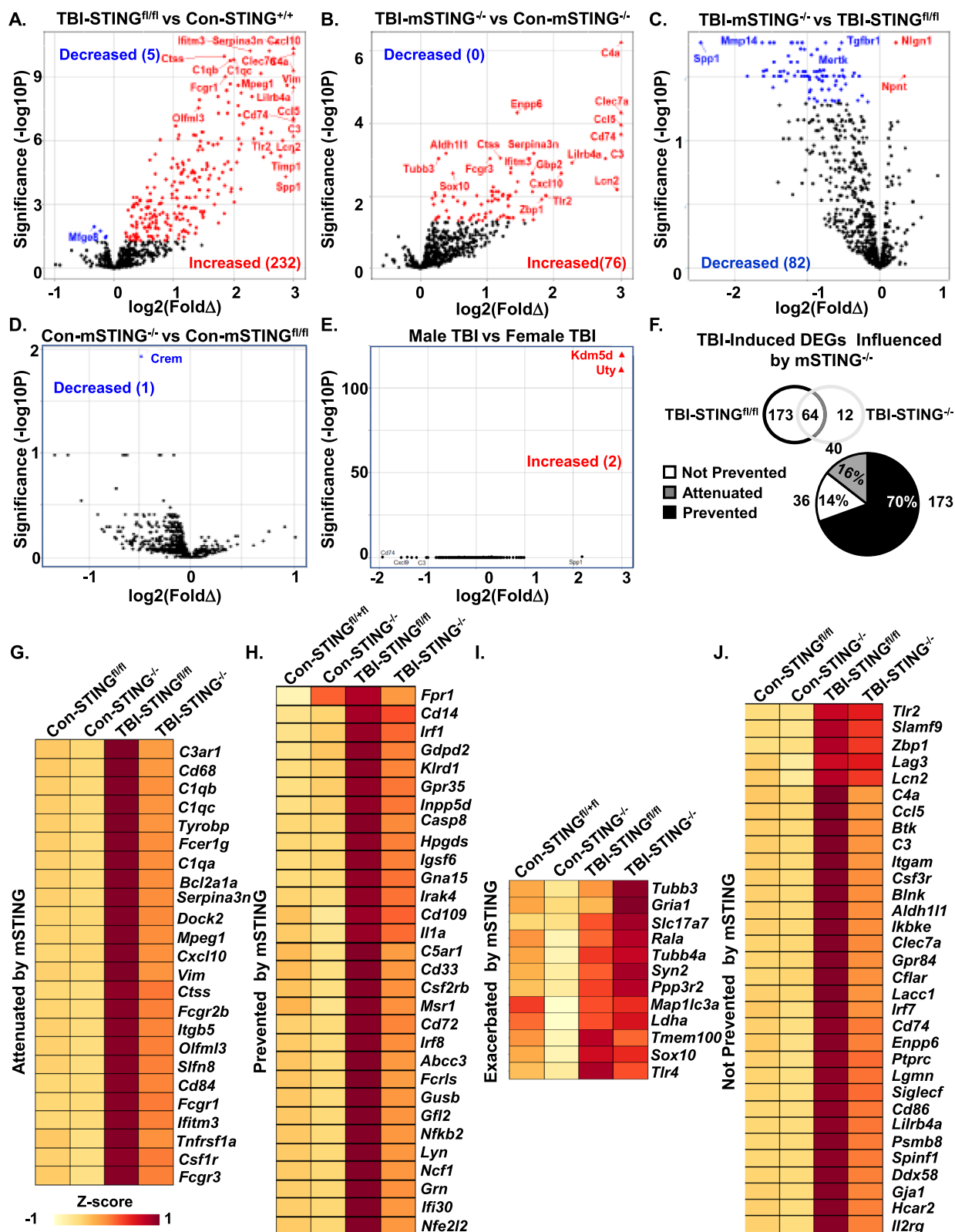


Fig. 3 (See legend on previous page.)

TBI-induced cognitive deficits 7 dpi were IFNAR1 independent

Another aspect of the cGAS-STING pathway is the interferon- α/β receptor 1 (IFNAR1), which is the primary receptor for type I interferons, alpha and beta [49–51]. These pathways were apparent in the NanoString analyses at 7 dpi in the cortex (Fig. 4). Thus, we next examined cognition and inflammation in male global IFNAR1^{-/-} mice. These mice were subjected to control or TBI (mFPI) and cortical and hippocampal-mediated cognition was assessed 7 dpi using NOR/NOL (Fig. 6A–F). There were no differences in total time exploring the objects between groups (Fig. 6B). Figure 6C, D show there were TBI-induced deficits in NOR 6 dpi with reduced time exploring the novel object and impairments in the discrimination index (TBI, $F_{1,20}=20.83$, $p<0.001$), which were independent of IFNAR1. These effects were mirrored in the NOL task 7 dpi (Fig. 6E–G). Time spent with the object in the novel location and discrimination index were reduced by TBI ($F_{1,20}=70.15$, $p<0.0001$, Fig. 6E–G), but again these effects were independent of IFNAR1.

After completion of the NOR/NOL cognitive assessments, cortices were extracted 7 dpi for RNA analyses. TBI increased interferon receptor-related *Irf7* expression, and this increase was dependent on IFNAR1 (Interaction, $F_{1,20}=p<0.0017$, Fig. 6H). Post-hoc analysis confirmed that *Irf7* expression was highest in the TBI-WT group compared to all other groups ($p<0.0001$, Fig. 6H). These *Irf7* data are consistent with the global knockout of IFNAR1. Moreover, several genes associated with inflammation (*Tnf*, *Gfap*, *H2-eb1*) were increased in the cortex 7 dpi (TBI, $F_{1,18}=7.92$, $p<0.05$, for each, Fig. 6I–K) but were independent of IFNAR1. Collectively, TBI-associated cognitive deficits and inflammatory mRNA expression in the cortex 7 dpi were independent of IFNAR1.

Single nucleus RNA-sequencing of cortical neurons 7 days after TBI

In this study, we aimed to determine the degree to which TBI-associated reduction in neuronal homeostasis were dependent on STING signaling in microglia. Thus, single nucleus RNA-sequencing (snRNA-seq) was conducted in cortical samples after control or TBI (7 dpi) in male and female STING^{fl/fl} or mSTING^{-/-} mice. Cortices were

dissected, nuclei were isolated, fixed, and barcoded at 7 dpi (Fig. 7A). Figure 7B shows that 89,320 nuclei were clustered into twenty distinct clusters. Clusters were identified based on gene expression of distinct markers (Fig. 7C–E) (*Syt1*-neurons, *Slc1a3*-astrocytes, *Mag*-oligodendrocytes, *Flt1*-endothelia, and *Csf1r*-microglia). In line with previous work using snRNA-seq, 90% of cells detected in Fig. 7D were neurons [22, 52, 53]. Notably, there were only a limited number of microglia resolved in this snRNAseq data set. Therefore, there were too few DEGs to delineate the profile of these cortical microglia 7 dpi. The focus here was to delineate the neuronal profile with TBI and mSTING^{-/-}. Thus, cortical neurons were subset and re-clustered (Fig. 7F) using existing gene markers (*Slc17a7*, *Cux1/2*, *Rorb*, *Gad1/2*, *Foxp2*, *Adarb2*) to classify the neuronal populations (Fig. 7G, I). The distribution of cells based on the four experimental groups is shown (Fig. 7H). Overall, there were approximately 80,000 nuclei collected from *Syt1*⁺ cortical neurons 7 dpi, and these nuclei were represented in all the experimental groups.

Ablation of microglial STING attenuated the response to TBI in cortical neurons

Continuing with the snRNA-seq analyses of *Syt1*⁺ cortical neurons 7 dpi, the pie chart (Fig. 8A) shows the distribution of specific neuronal profiles resolved. Here, 36% of the *Syt1*⁺ nuclei corresponded to upper layer neurons (*Cux1/2*⁺), 30% of the *Syt1*⁺ nuclei corresponded to layer 4 neurons (*Rorb*⁺), 21% of the *Syt1*⁺ nuclei corresponded to deep layer neurons (*Foxp2*⁺), and 13% *Syt1*⁺ nuclei corresponded to inhibitory neurons (*Gad1/2*⁺). These neuronal sub-clusters were used for analyses. Figure 8B highlights that TBI resulted in both increased and decreased mRNA expression in cortical neurons 7 dpi, with more overall suppression of gene expression. For upper layer neurons, there were 1,146 DEGs ($p\text{-adj}<0.05$), with 697 increased and 449 decreased DEGs after TBI. Moreover, the influence of TBI on these upper layer neurons was 50% dependent on mSTING (600 DEGs, Fig. 8C). For layer 4 neurons, there were 749 DEGs ($p\text{-adj}<0.05$) with 227 increased and 522 decreased DEGs after TBI. The influence of TBI on layer 4 neurons was 45% dependent on

(See figure on next page.)

Fig. 4 Canonical pathways associated with inflammation and IFN signaling 7 dpi were attenuated by mSTING^{-/-}. Continuing with the NanoString experiment outlined in Fig. 3, Ingenuity Pathway Analysis (IPA) assessed canonical pathways, master regulators, and upstream regulators influenced by TBI and mSTING^{-/-} (z-score). **A** Heat map of IPA canonical pathways induced by TBI. **B** Heat map of IPA canonical pathways induced by TBI and prevented by mSTING^{-/-}. **C** Heat maps of activated or inhibited master regulators by TBI. **D** Heat map of activated or inhibited master regulators by TBI and prevented by mSTING^{-/-}. **E** Heat map of activated or inhibited IPA upstream regulators induced by TBI. **F** Heat map of IPA upstream regulators induced by TBI and prevented by mSTING^{-/-}. Values were significant with a $p\text{-adj}<0.05$

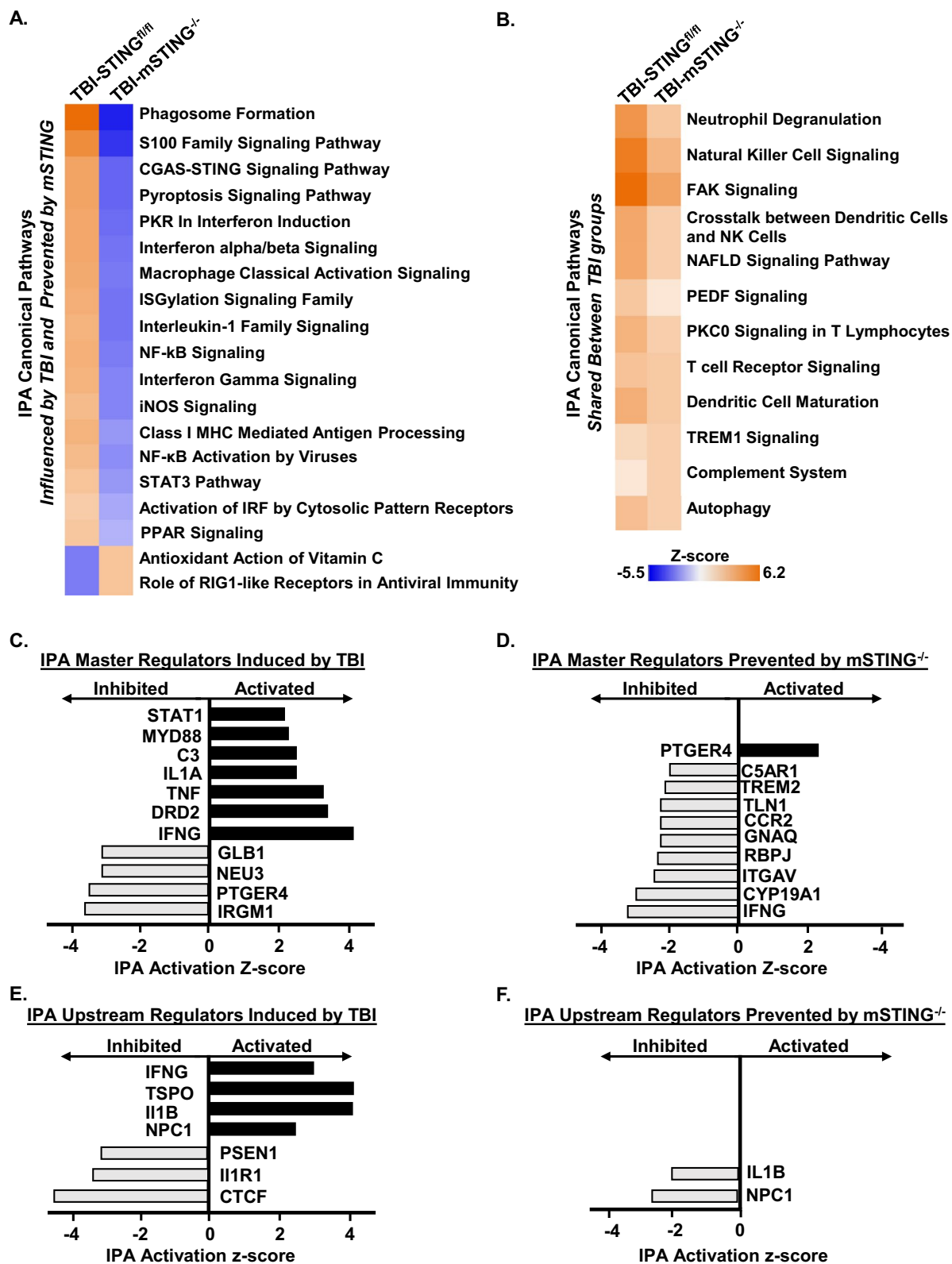


Fig. 4 (See legend on previous page.)

mSTING (357 DEGs, Fig. 8C). For deep layer neurons, there were 1104 DEGs (p -adj < 0.05) after TBI with 445 increased and 659 decreased DEGs. The influence of TBI on deep layer neurons was 47% dependent on mSTING (591 DEGs). Last, there were 241 DEGs (p -adj < 0.05) in the inhibitory neurons with 49 increased and 192 decreased. In inhibitory neurons, the influence of TBI was 64% dependent on mSTING for 154 DEGs (p -adj < 0.05, Fig. 8C). Thus, there was a robust effect of TBI on cortical neurons 7 dpi and about 50% of the DEGs were prevented by mSTING^{-/-}.

Notably, both male and female mice were included in these snRNA-seq studies. Although these studies were not appropriately powered to make comparisons based on sex, we examined male and female mice within the TBI-STING^{fl/fl} group. The top DEGs are shown in the dot plot for male TBI versus female TBI functional wild type mice (Fig. 8C). *Xist* was increased in female wild type TBI mice compared to males and this is an X linked gene [54]. *Uty*, *Eif2s3y*, *Kdm5d*, and *Dxd3y* were increased in male TBI mice compared to female TBI mice. These genes are all y-linked [44, 55, 56]. Thus, male and female snRNA-seq data were analyzed together.

To visualize the significant DEGs in Fig. 8B, C, volcano plots are shown (Fig. 8E–J). For upper layer neurons (UL), the volcano plot shows the comparison between Con-STING^{fl/fl} and TBI-STING^{fl/fl} mice with 697 DEGs increased and 449 DEGs decreased (p -adj < 0.05, Fig. 8E). For instance, there was a TBI associated reduction in two synaptic plasticity related genes,

Arc and *Homer1*. Figure 8F shows the comparison between Con-mSTING^{-/-} and TBI-mSTING^{-/-} mice. In this comparison, 1728 DEGs were increased by TBI and 1312 DEGs were decreased. Figure 8G shows comparison between TBI-mSTING^{-/-} and TBI-STING^{fl/fl} mice. Here, there were 44 DEGs increased and 148 DEGs decreased. These data highlight a reduced influence of TBI on upper layer cortical neurons in the mSTING^{-/-} mice compared to controls (STING^{fl/fl} mice). For instance, the reduction

of *Homer1* and *Arc* after TBI were prevented in the TBI-mSTING^{-/-} group.

For deep layer neurons (DL), the volcano plot shows comparisons between Con-STING^{fl/fl} and TBI-STING^{fl/fl} mice with 445 DEGs increased and 659 DEGs decreased (p -adj < 0.05, Fig. 8H). For instance, there was a TBI associated reduction in three synaptic plasticity-related genes, *Arc*, *Bdnf*, and *Homer1*. Reductions also evident in *ApoE* (lipid transport), *Calm1* (calcium signaling), and *Atg4a* (autophagy). Figure 8I shows the comparison between Con-mSTING^{-/-} and TBI-mSTING^{-/-} mice. There were 924 DEGs increased and 1662 DEGs decreased. These data highlight that there was a reduced influence of TBI on deep layer cortical neurons in the mSTING^{-/-} mice compared to controls (STING^{fl/fl}). For instance, the reduction of *Atg4a* and *Homer1* after TBI were prevented in the TBI-mSTING^{-/-} group (Fig. 8J). Overall, TBI had a suppressive effect on cortical neurons that was influenced by microglial STING.

Ablation of microglial STING attenuated TBI-induced imbalance in neuronal homeostasis of cortical neurons

Next, *Syt1*⁺ cortical neurons 7 dpi, DEGs (p -adj < 0.05) were analyzed in IPA for canonical pathways, master regulators and upstream regulators. Significant canonical pathways (z score, -3.8 to 3.9) influenced by TBI are shown in upper layer (UL), layer 4 (L4), deep layer (DL) and inhibitory (IN) cortical neurons (Fig. 9A). These pathways were conserved across the four neuronal subtypes. For example, TBI increased canonical pathways associated with neuronal restructuring (e.g., Cilium Assembly, VDR/RXR Activation, RHOGDI Signaling, Transcriptional Regulation by MECP2, and Netrin Signaling) and inhibition of growth (PTEN signaling). TBI also suppressed canonical pathways associated with neuronal homeostasis and metabolism (CREB Signaling, Synaptogenesis, S100 Family Signaling). These data are consistent with our previous work on the effects of TBI on neurons [11, 22]. Next the significant canonical

(See figure on next page.)

Fig. 5 TBI-induced neuronal injury and cognitive deficits 7 dpi were mSTING dependent. **A** Male and female functional wild type (STING^{fl/fl}) and CX₃CR1/STING^{-/-} (mSTING^{-/-}) mice were subjected to midline fluid percussion injury or left as uninjured controls. Several parameters of neuronal injury were assessed in the cortex and plasma 7 dpi. **A** Representative images of NeuN⁺ labeling (10x) in the cortex 7 dpi. White box represents location where inset was selected. Right panel shows enlarged labeling from inset. **B** Percent-area of NeuN⁺ labeling per 10x field in the medial cortex 7 dpi (n = 6–8). **C** Representative images of lipofuscin autofluorescence and NeuN⁺ labeling in the lateral cortex 7 dpi. Insets show enlarged images of lipofuscin auto-fluorescence in NeuN⁺ cells. **D** Quantification of lipofuscin foci in NeuN⁺ neurons in the lateral cortex 7 dpi. **E** Neurofilament light chain protein (NF-L) was determined in the plasma 7 dpi (n = 6–8). In a separate study, cognition was determined using the novel object recognition (NOR) and location (NOL) tests (n = 12–16). **F** Total exploration time (seconds) of the objects in NOR. **G** Percent time exploring the novel object. **H** Discrimination index of time exploring the novel object. **I** Total exploration time (seconds) of the objects in NOL. **J** Percent time exploring the object in the novel location. **F** Discrimination index of time exploring the object in the novel location. Bars represent the mean ± SEM and individual data points are provided. Means with (*) are significantly different from control groups (p < 0.05). Means with (^) tend to be different from control groups (p = 0.06–0.1)

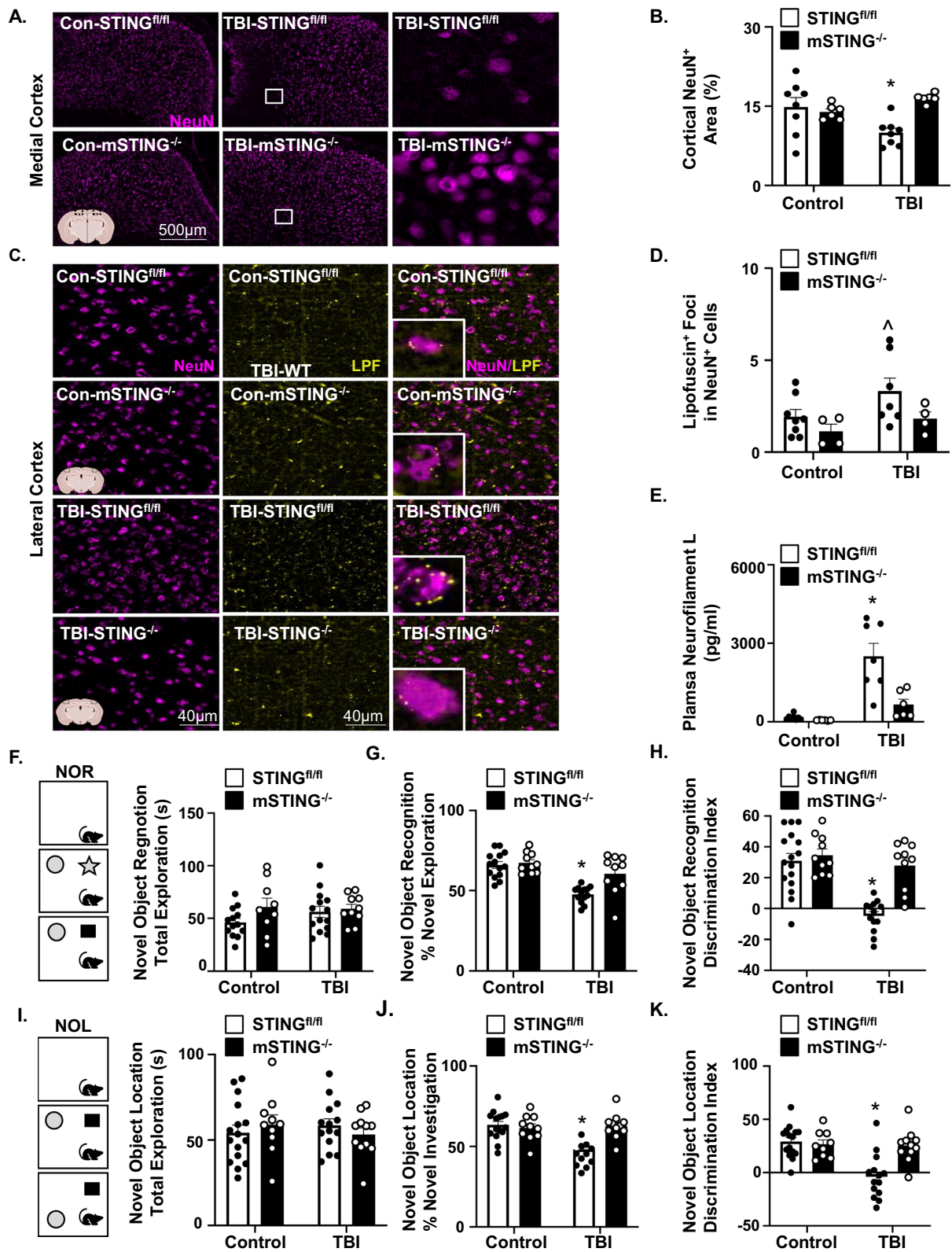


Fig. 5 (See legend on previous page.)

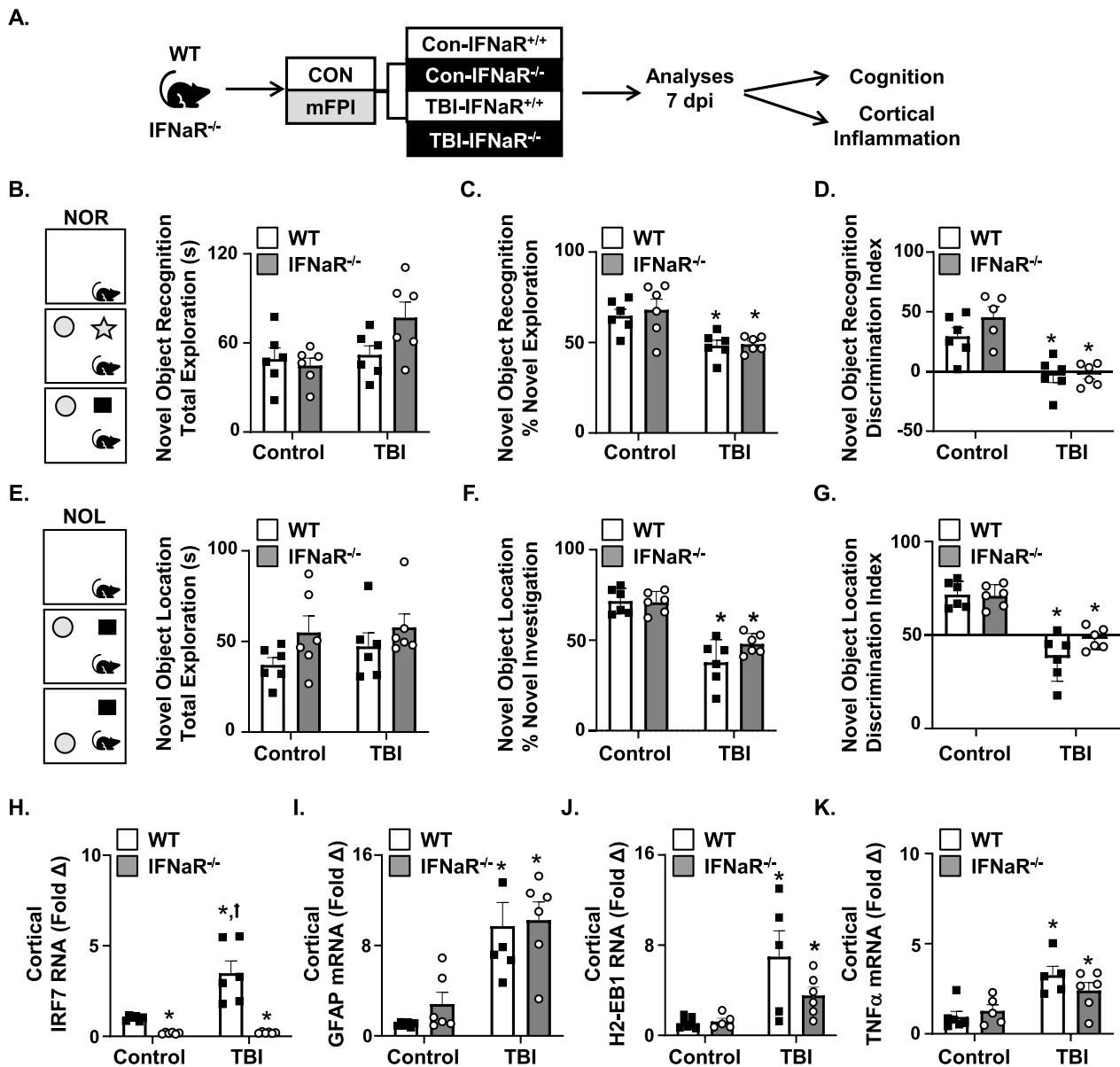


Fig. 6 TBI-induced cognitive deficits 7 dpi were IFNAR1 independent. **A** Wildtype (IFNAR1^{+/+}) and global IFNAR1 knockout (IFNAR1^{-/-}) male mice were subjected to midline fluid percussion injury (TBI) or left as uninjured controls. Cognition (novel object recognition (NOR) and location (NOL)) and cortical inflammation were assessed 7 dpi (n = 5–6). **B** Total exploration time (seconds) of the objects in NOR. **C** Percent time exploring the novel object and **D** Discrimination index of time exploring the novel object. **E** Total exploration time (seconds) of the objects in NOL. **F** Percent time exploring the object in the novel location. **G** Discrimination index of time exploring the object in the novel location. From the same mice, mRNA levels of **(H)** *Irf7*, **(I)** *Gfap*, **(J)** *H2-Eb1*, and **(K)** *Tnf* were determined from the cortex (n = 5–6). Bars represent the mean ± SEM, and individual data points are provided. Means with (*) are significantly different from control groups (p < 0.05) and means with (†) are significantly different from all other groups (p < 0.05)

pathways induced by TBI and prevented by mSTING are shown in upper layer (UL), layer 4 (L4), deep layer (DL) and inhibitory (IN) cortical neurons (Fig. 9B). Canonical pathways that were decreased following TBI and influenced by mSTING were associated with neuronal health (Oxytocin Signaling, Endothelin-1 Signaling, CREB

Signaling, and Orexin Signaling). Canonical pathways that were increased by TBI and influenced by mSTING (Fig. 9B) were associated with neuronal restructuring (Cilium Assembly) and inhibition of growth (PTEN).

Next, significant master regulators that were influenced by TBI are shown in upper layer (UL), layer 4 (L4), deep

layer (DL) and inhibitory (IN) cortical neurons (Fig. 9C). TBI increased DLGAP3, MYCBP2, RELN, CDK5 in upper layer and layer 4 neurons, and decreased CAMK, CREM, IL-4R, and GRM5. Master regulators reduced by TBI associated with neuronal homeostasis (e.g., CAM4K, CREM, IL4R, GRM5, ADORA2A) were prevented by mSTING, especially in deep layer neurons (Fig. 9D). As such, deep layer neurons had the most master regulators prevented by mSTING^{-/-} (7). Upper layer neurons had the most upstream regulators induced by TBI and prevented by mSTING^{-/-} (7). These upstream regulators are associated with neuronal homeostasis (e.g., MECP2, MKNK1, CREB1, IL4R, CREM, ADORA2A, BDNF). These regulators were reduced by TBI, and this reduction was prevented by mSTING^{-/-} (Fig. 9F). Upstream regulators increased by TBI include HNRNPU, PTF1A, FMR1, and MAPT and decreased upstream regulators include BDNF, IL4R, CREM, and CREB1 (Fig. 9E). These changes were prevented by mSTING, especially in upper layer cortical neurons (Fig. 9F). Taken together, TBI reduced cortical neuronal homeostasis 7 dpi and this was dependent on microglial STING.

Discussion

We previously reported that a global knockout of the stimulator of interferons genes (STING) reduced neuroinflammation (7 and 30 dpi) and cognitive impairment associated with diffuse TBI [22]. Thus, the aim of this study was to determine the degree to which a microglia-specific knockout of STING influenced neuroinflammation, neuronal dysfunction, and cognitive deficits induced by diffuse TBI. Here, TBI induced microglial morphological restructuring and cortical inflammation 7 dpi were mSTING dependent. In addition, neuronal injury and cognitive impairment 7 dpi were also dependent on mSTING. With snRNA-seq of cortical neurons after TBI, there were reductions in CREB signaling, synaptogenesis, and oxytocin signaling and increases in cilium assembly and PTEN signaling. These reductions in neuronal homeostasis were mSTING dependent. Collectively, ablation of STING in microglia attenuated

TBI-induced interferon responses, cortical inflammation, cortical pathology, neuronal dysfunction, and cognitive impairment.

One key finding of this study was that increased STING expression 7 days after TBI in the cortex was localized to IBA1⁺ microglia, and this increase in STING was ablated by microglial STING^{-/-}. The increase in STING expression in the cortex after TBI is consistent with previous findings showing enhanced IFN-I responses after either diffuse [11, 15, 16, 22, 51] or penetrating TBI [27, 28, 50, 57]. Moreover, studies of penetrating TBI induced by controlled cortical impact (CCI) indicate that STING is localized to IBA1⁺ microglia [27, 28, 57]. The extension here is that STING was localized to cortical microglia after diffuse TBI and this increase was ablated by a selective knockout of STING in microglia. At baseline, STING signaling is present at low-levels in the brain, but capable of rapidly responding following injury [22]. Notably, STING induction was detected in other cell types including neurons, astrocytes, and peripheral immune cells after penetrating TBI [27, 28, 57, 58]. Here, histological analyses show that STING was localized in cortical microglia and undetectable in astrocytes and neurons after diffuse TBI. Nonetheless, it is plausible that STING is increased myriad cell types after TBI and that injury type, severity, and time after injury influence the cellular distribution of STING. Assessment of mRNA from percoll enriched microglia paralleled the histological data with a TBI-dependent increase in STING mRNA 7 dpi and ablation by microglial STING^{-/-}. These findings are also consistent with our previous reports using snRNA-seq that microglia, not neurons, expressed genes associated with the production of IFN-I after TBI [22]. These RNA and protein findings validate the targeted knock out of STING in microglia. Overall, TBI increased STING expression within IBA1⁺ microglia 7 dpi was ablated in mSTING^{-/-} mice.

Another relevant point is that TBI-induced microglial restructuring (IBA1⁺ percent area increase) 7 dpi was dependent on mSTING. Rod-shaped microglia and GFAP⁺ astrocytes were also increased 7 dpi, but were

(See figure on next page.)

Fig. 7 Single nucleus RNA-sequencing of cortical neurons 7 days after TBI. **A** Male and female functional wild type (STING^{fl/fl}) and CX₃CR1/STING^{-/-} (mSTING^{-/-}) mice were subjected to midline fluid percussion injury or left as uninjured controls. At 7 dpi, mice were sacrificed, and cortices were dissected, pooled (3 males, 3 females per group), and nuclei were collected. RNA profiles of collected nuclei were determined 7 dpi using snRNA-sequencing. Clustering and differential expression were determined using Seurat in R. **B** UMAP plots indicate 19 distinct clusters of cortical cells based on identity genes. **C** and **E** Clusters were identified based on established gene expression: neurons (*Syt1*), oligodendrocytes (*Mag*), microglia (*Csf1r*), astrocytes (*Slc1a3*) and endothelia (*Flt1*). Dot plot figure shows gene expression of identifying genes for clusters. **D** Representative percentage of each cell type. Next, neurons (*Syt1*+) were subset and re-clustered. **F** The UMAP plot shows that 14 clusters of cortical neurons identified. **G** and **I** Dot plot figure shows gene expression of identifying genes for clusters based established gene expression: upper layer neurons (*Cux2*), layer 4 neurons (*Rorb*), deep layer neurons (*Foxp2*), and inhibitory neurons (*Gad1*). **H** The UMAP plot shows the distribution of cortical neuron clusters between the experimental groups

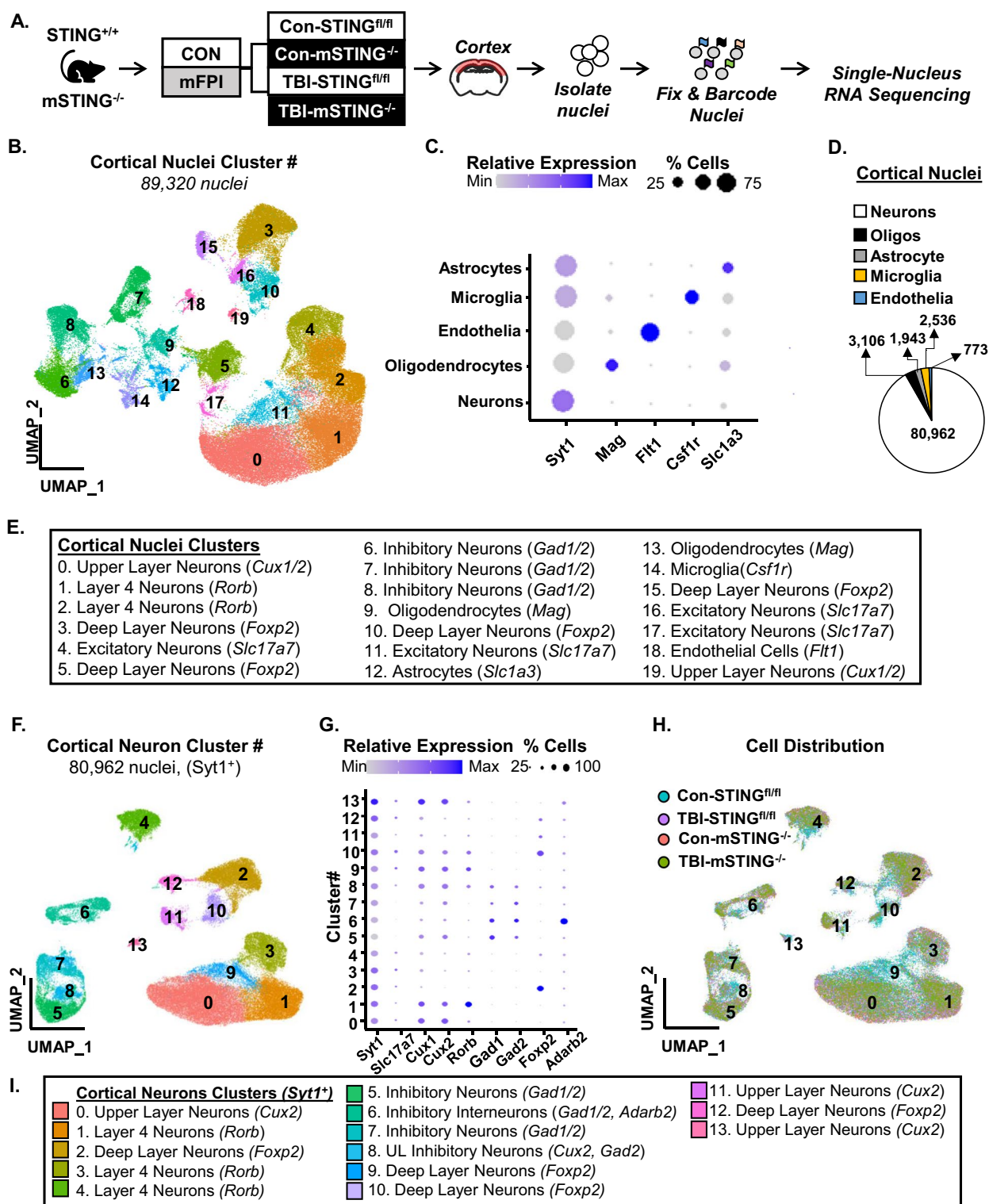


Fig. 7 (See legend on previous page.)

independent of mSTING^{-/-}. These data are like our previous reports where TBI-induced microglial restructuring was reduced by global STING^{-/-}, but astroglia

was unaffected [22]. Similarly, another report showed that astrocytes were unresponsive to DMXAA, a STING agonist after TBI [16]. Diffuse TBI does not significantly

influence microglial proliferation [11, 39]. Thus, increase in the percent area of IBA in the cortex 7 dpi is attributed to morphological restructuring of microglia. Rod-shaped microglia are detected in humans and rodents in the context of advanced age, neurodegeneration, and TBI [12, 42, 59], but their function is unclear. In a previous report, rod-shaped microglia were reduced in the cortex 7 dpi of global *STING*^{-/-} mice [22]. Here, rod-shaped microglia were unaffected by *mSTING*^{-/-}. One explanation for this difference is that rod-shaped microglia in the cortex 7 dpi are *mSTING* independent and may serve a neuroprotective role. For instance, these structurally unique and elongated microglia aligned with apical dendrites of damaged neurons in the cortex 7 dpi [12]. These cells were present 7 dpi in the cortex of mice with microglia depletion (PLX5622), which was associated with reduced neuroinflammation and cognitive improvement [11]. Furthermore, elimination of rod-shaped microglia using a *TREM2* knock out in an ALS model increased neuronal hyperactivity, worsened motor deficits, and further reduced survival rates in mice [60]. Collectively, there were structurally divergent profiles of cortical glia 7 dpi and the reactive microglia profile was attenuated by *mSTING*^{-/-}.

Another point for discussion is the increased IFN-I and pro-inflammatory signaling in the cortex 7 dpi was dependent on microglial *STING*. For example, there were 232 genes detected in the NanoString panel (770 genes) associated with type I interferon signaling, inflammation, and antigen presentation 7 dpi. A majority of these TBI-associated genes were reduced (86%) by *mSTING*^{-/-}. Notably, there were minimal sex and genotype-control differences detected in the cortical mRNA analyses. For instance, there were only two sex-linked genes (*Kdm5d* and *Uty*) [44, 55] different between male and female TBI mice and only one gene (*Crem*) different between control-*mSTING*^{-/-} and control-*mSTING*^{fl/fl} mice. Overall, TBI increased genes associated with IFN-I and inflammation in male and female mice, and these were reduced by *mSTING*^{-/-}. Consistent with these DEGs, IPA canonical pathways and master regulator analyses showed

myriad IFN-I and inflammatory pathways increased after TBI including activation of IRE, NFκB, phagosome formation, and cGAS-*STING*. These increases in genes and pathways associated with IFN-I, inflammation, phagocytosis, and microglial priming are consistent with previous reports 7 dpi [12, 16, 22]. Key pathways induced by TBI 7 dpi and prevented by *mSTING*^{-/-} included cGAS-*STING*, NF-κB, and neuroinflammation signaling. Notably, some DEGs (35) and IPA pathways that were induced by TBI were unaffected by *mSTING*^{-/-}. These DEGs were genes associated with the complement cascade (*C3*, *C4a*), astrocyte associated genes (*Aldh1l1*, *Gja1*) and endothelia associated genes (*Blnk*, *Enpp6*). There were 12 total genes uniquely increased by TBI in *mSTING*^{-/-} mice. A majority of these increased DEGs were neuronal (*Tubb3*, *Gria*, *Slc17a7*, *Rala*, etc.), and may represent improved neuroprotection following TBI in *mSTING*^{-/-} mice. Thus, the inflammatory and IFN-I responses in the cortex 7 dpi were robustly influenced by *STING* in microglia.

One notable finding of this study was that global *IFNAR1* knockout did not reduce cortical inflammation or cognitive impairment 7 dpi. We and others have shown increased genes and pathways following diffuse and penetrating TBI related to the *IFNAR1* pathway [11, 15–17, 22, 27, 28, 50, 51]. Presumably cGAS-*STING* activation in microglia after TBI increases *Irf3* and corresponding IFN-I that would use the *IFNAR1* [24, 61]. Indeed, several studies show improvements in inflammation, cognition, and neurologic dysfunction following selective modulation of the *IFNAR1* pathway with diffuse TBI acutely [51] and penetrating TBI both acutely and chronically [50]. Here, global *IFNAR1* knockout did not reduce cortical inflammation or cognitive impairment 7 dpi. Global *IFNAR1* knockout, however, reduced the induction of *Irf7* 7 dpi. One explanation is that the *STING* pathway also promotes NF-κB-mediated genes (e.g., *IL-6*, *TNF* and *IL-1*) [25, 26] and these pro-inflammatory cytokines are more responsible for the downstream effects on neurons and cognitive processes. For instance, the IL-1 receptor-1 (*IL1-R1*) is highly expressed

(See figure on next page.)

Fig. 8 Ablation of microglial *STING* attenuated the response to TBI in cortical neurons. **A** Continuing with the snRNA-seq experiment outlined in Fig. 7, the pie chart shows the percentages of different *Sty1*+ neurons. **B** The number of DEGs increased or decreased by TBI (*TBI-STING*^{fl/fl} vs *Con-STING*^{fl/fl}) for each cortical neuron cluster are shown. **C** The percentage and number of DEGs induced by TBI and prevented by *mSTING*^{-/-} (*TBI-STING*^{fl/fl} vs *TBI-mSTING*^{-/-}) in each neuronal cluster. **D** Dot plot shows the top DEGs between male and female *TBI-STING*^{fl/fl} mice. **E** Volcano plot of DEGs in the upper layer (UL) neurons of *TBI-STING*^{fl/fl} vs *Con-TBI*^{+/+}. **F** Volcano plot of DEGs in the upper layer (UL) neurons of *TBI-mSTING*^{-/-} vs *Con-mSTING*^{-/-}. **G** Volcano plot of DEGs in the upper layer (UL) neurons of *TBI-mSTING*^{-/-} vs *TBI-STING*^{fl/fl}. **H** Volcano plot of DEGs in the deep layer (DL) neurons of *TBI-STING*^{fl/fl} vs *Con-TBI*^{+/+}. **I** Volcano plot of DEGs in the deep layer (DL) neurons of *TBI-mSTING*^{-/-} vs *Con-mSTING*^{-/-}. **J** Volcano plot of DEGs in the deep layer (DL) neurons of *TBI-mSTING*^{-/-} vs *TBI-STING*^{fl/fl}. Red dots represent genes significantly increased with $|\log_2\text{FoldChange}| > 0$ and $p\text{-adj} < 0.05$. Blue dots represent genes significantly decreased with $|\log_2\text{FoldChange}| > 0$ and $p\text{-adj} < 0.05$. Values were significant with a $p\text{-adj} < 0.05$

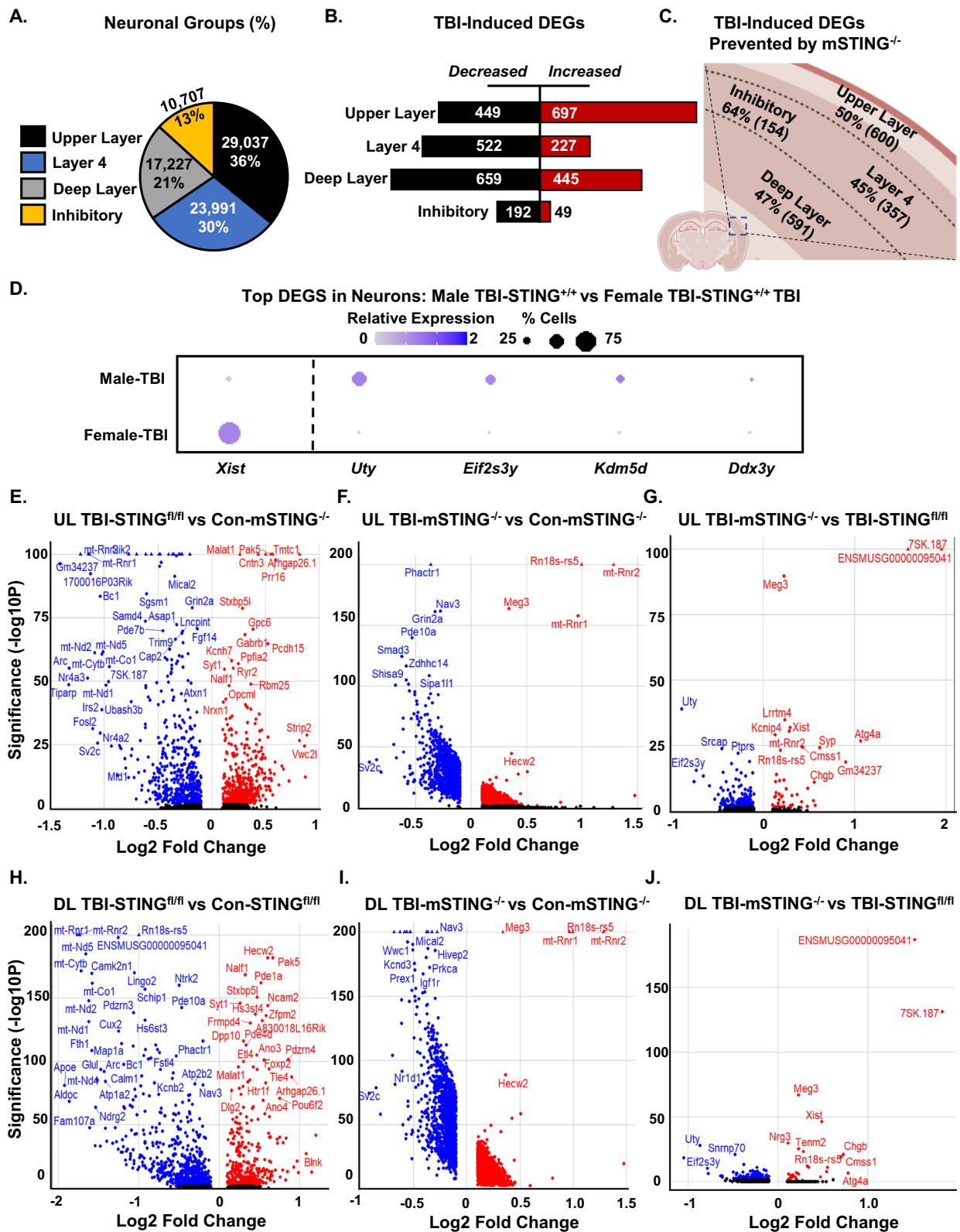


Fig. 8 (See legend on previous page.)

on DG neurons of the hippocampus [52, 62] and IL-1/IL-R1 responses are evident chronically after closed head TBI [63]. Another explanation is that there are reported confounds of IFNAR1^{-/-}. For instance, one report showed that global and microglia specific knockouts of IFNAR1 led to dysfunctional microglia with a “bubble” phagosome formation and increased accumulation of DNA-damaged neurons [64]. Another study showed that astrocytic IFNAR1 deletion in mice caused cognitive dysfunction and reduced synaptic plasticity [65]. Because of the potential confounds of these global IFNAR1^{-/-} mice, we conducted only limited studies with them using only male mice and instead focused on mSTING^{-/-} mice. Taken together, the interpretation is that ablating STING in microglia was more beneficial than targeting IFNAR1 because STING is upstream and thus affects both IFN- γ and NF- κ B mediated responses after diffuse TBI.

Another relevant finding was the neuropathological influences of TBI (7 dpi) were dependent on STING in microglia. For example, there was reduced percent area labeling of NeuN⁺ in the cortex 7 dpi, which was attenuated in TBI-mSTING mice. The interpretation is that reduced NeuN⁺ labeling corresponds with more dysfunction or atypical neurons in the cortex after diffuse TBI. A similar TBI-induced reduction of NeuN in the cortex 7 dpi was detected in a weight drop model of TBI in mice (up to 6 months later) and associated with increase blood brain barrier permeability after TBI [45]. In the same study, the reduced NeuN⁺ neurons were associated with reduced synaptic plasticity [45]. Parallel to this, lipofuscin (i.e., autofluorescent lipid debris) detected here in cortical neurons may also represent reduced homeostasis [66]. Indeed, several studies show increased lipofuscin in the brain with age or after TBI [36, 46]. Moreover, increased lipofuscin after TBI in aged mice was associated with neuronal loss, glial activation, and oxidative stress [46]. Taken together, targeted mSTING deletion prevented inflammatory cytokine, chemokine, and IFN- γ production that deleteriously affected neuronal homeostasis in the cortex.

Consistent with the above data, novel data shows that the TBI-associated increase in plasma NF-L (7 dpi) was attenuated in the TBI-mSTING^{-/-} mice. NF-L is a

clinically validated biomarker for neuronal and axonal injury after moderate to severe TBI in humans [48, 67]. Moreover, use of plasma NF-L as a biomarker to represent neuropathology in humans has been validating using MRI and cerebral microdialysis [48]. Thus, we interpret the data to show ablating STING in microglia was neuroprotective with less axonal and neuronal damage after diffuse TBI. Non-selectively inhibition of microglia after CNS injury may have off target effects that worsen recovery. For instance, minocycline reduced microglia activation in humans (by MRI) after TBI, but increased the neuronal damage marker, NF-L, in the plasma [68]. Furthermore, depletion of microglia prior to spinal cord injury worsened pathology by interfering with astrocytic dynamics [69]. Thus, inhibition of specific microglia pathways, like STING, are critical for addressing chronic neuroinflammation elicited by traumatic CNS injury while minimizing off target effects of intervention. Parallel with the evidence of increased neuronal injury 7 dpi, TBI reduced cortical/hippocampal dependent memory with reduced novel object/exploration 7 dpi. Here, novel data shows that these reductions in cognition after TBI were mSTING dependent. These data are consistent with previous studies of global STING^{-/-} [22] and microglial elimination [11] demonstrating that limiting inflammatory pathways in microglia improved behavioral and cognitive recovery after diffuse TBI. Taken together, TBI promoted neuronal and cognitive dysfunction 7 dpi in an mSTING dependent manner.

Consistent with our previous data [11, 22] snRNA-seq analysis in the cortex 7 dpi shows suppression of neuronal pathways associated with metabolism and homeostasis (CREB Signaling in Neurons, Synaptogenesis, S100 Signaling, GPCR Mediated Nutrient Sensing, and Cholecystokinin Signaling). This pattern was conserved across all neuronal subtypes sampled, especially the excitatory neurons (DL, L4, and UL) indicating a shared pattern of cortical neuron suppression. Here, novel data shows that STING ablation in microglia prevented these imbalances. For instance, approximately 50% of all DEGs influenced by TBI were prevented in microglial mSTING^{-/-} mice. The mSTING dependent reversals of the TBI effects in upper layer (UL), layer 4 (L4), and deep layer (DL)

(See figure on next page.)

Fig. 9 Ablation of microglial STING attenuated TBI-induced imbalance in neuronal homeostasis of cortical neurons. Continuing with the snRNA-seq experiment outlined in Figs. 7 and 8. Ingenuity Pathway Analysis (IPA) assessed canonical pathways, master regulators, and upstream regulators influenced by TBI and mSTING^{-/-} in upper layer neurons (UL), layer 4 neurons (L4), deep layer neurons (DL), and inhibitory neurons (IN). **A** Heat map of IPA canonical pathways induced by TBI (TBI vs Con-STING^{fl/fl}) are shown. **B** Heat map of IPA canonical pathways induced by TBI and prevented by mSTING^{-/-} are shown. **C** Heat maps of activated or inhibited IPA master regulators by TBI (TBI vs Con-STING^{fl/fl}). **D** Heat map of activated or inhibited IPA master regulators by TBI and prevented by mSTING^{-/-} are shown. **E** Heat map of activated or inhibited IPA upstream regulators induced by TBI are shown. Values were significant with a p -adj < 0.05

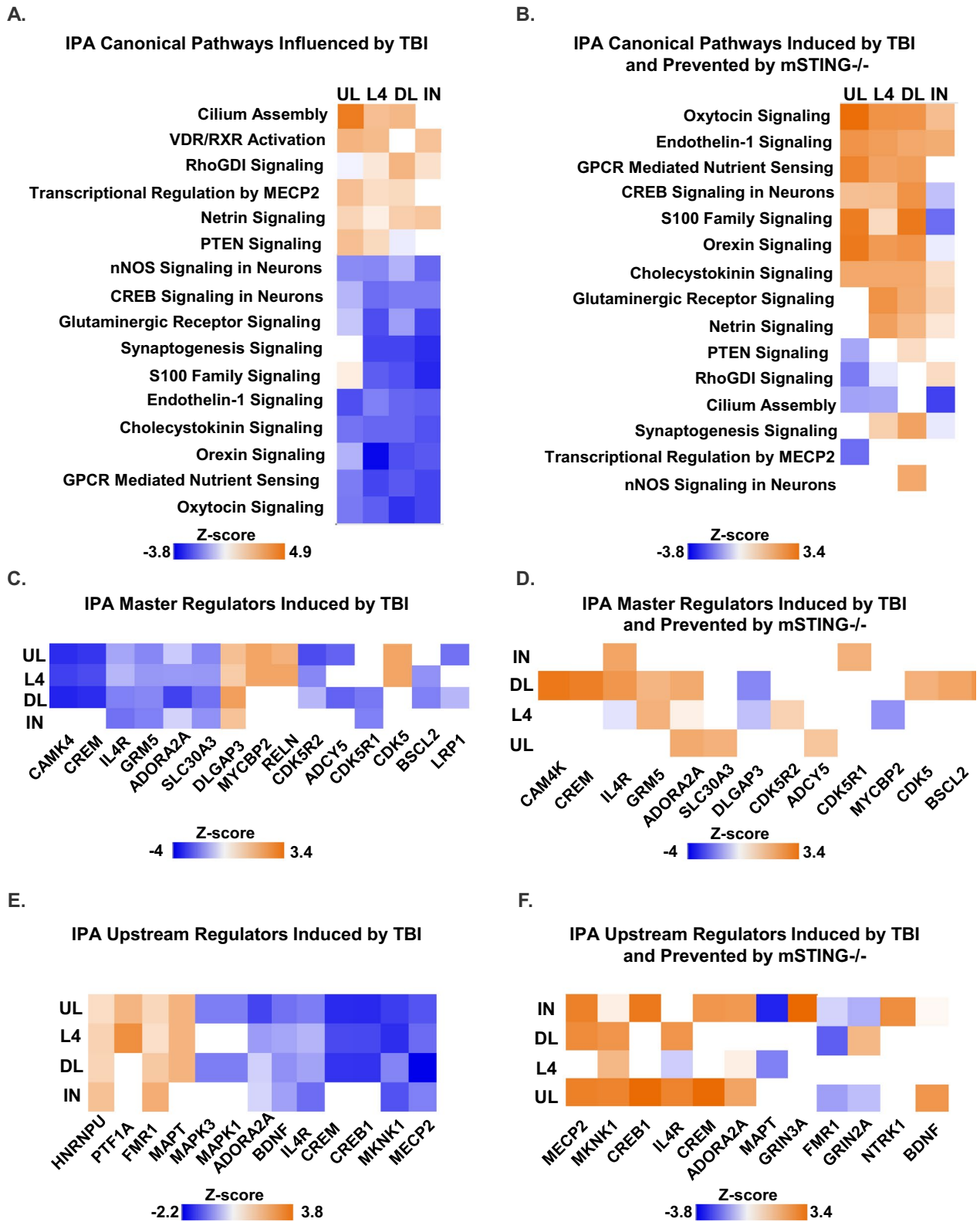


Fig. 9 (See legend on previous page.)

neurons included canonical pathways (Cilium Assembly, RHODI, and Netrin Signaling) and master regulators (HNRNPU, PTF1A, FMR1, MAPT) associated with neuronal restructuring. These RNA data are consistent with the physiological neuronal restructuring and dendritic atrophy detected after TBI [11]. These physiological changes reported after TBI in mice were associated with cognitive dysfunction and depressive-like behavior [10, 11]. In addition, the mSTING dependent reversals of the TBI effects in UL, L4, and DL neurons included canonical pathways (Oxytocin Signaling, GPCR Mediated Nutrient Sensing, CREB Signaling, S100 Family Signaling) and master regulators (MECP2, CREB1, IL4R, and BDNF) associated with neuronal homeostasis and metabolism. These pathways and master regulators increased following TBI are related to neuronal and synaptic remodeling, and likely represent the same cassette of genes previously reported to be associated with the Phosphatase and Tensin Homolog (PTEN) signaling [22]. PTEN is a master regulator of neuronal and dendritic morphological restructuring [70], and the increase in PTEN following traumatic CNS injuries is a potential target of intervention [71, 72]. In summary, the reduced homeostasis of cortical neurons 7 dpi was associated with increased STING responses in microglia.

A final point for discussion is that this study was not powered for sex comparisons. Nonetheless, male and female mice were used and there were similar patterns of responses following TBI. For instance, NanoString and single nucleus RNA-seq analyses revealed the same sex-linked genes (*Uty*, *Kdm5d*) were the top DEGs between male and female mice 7 dpi. Again, sex differences in TBI is an important issue and several reports indicate sexually dimorphic responses following TBI [73–76]. Nonetheless, STING and IFN-I responses to diffuse TBI were conserved in male and females 7 dpi. In conclusion, while sex differences are important aspects to interrogate with TBI, STING, and IFN-I responses after diffuse TBI were conserved in males and females.

Of note, we used the CX3CR1-Cre/ERT2 x STING^{fl/fl} breeding pairs to generate our knockout (mSTING^{-/-}) and our wild type (mSTING^{fl/fl}) mice following administration of tamoxifen. This Cre-driver allows for moderately high specificity, low leakiness, and high efficiency of recombination [30, 31]. Notably, the design of the CX3CR1-Cre/ERT2 construct results in CX3CR1 heterozygosity in Cre-positive mice. CX3CR1 regulates the activation of microglia. CX3CR1-CreERT homozygous mice would be more of a concern than CX3CR1-CreERT heterozygous based on other studies showing worsen recovery following brain injury or LPS challenges [77–79]. It is important to highlight that no behavioral, glial, or inflammatory differences were detected between the

Con-mSTING^{-/-} and Con-STING^{fl/fl} mice. Additionally, CX3CR1 was not a differentially expressed gene following TBI. Last, the mSTING^{-/-} data we report here parallel and support our previous published data using a global Sting KO. There is not an obvious confound of CX3CR1-CreERT heterozygous mice. Overall, STING and Type I IFN signaling are evident in the sub-acute time point after TBI and function to augment, inflammation, neuropathology and cognitive impairment.

In summary, we show that diffuse TBI induced a STING response in microglia associated with IFN-I that impaired cortical neuronal homeostasis and cognition. The TBI-induced neuronal restructuring, neuronal damage, and snRNA-profiles were dependent on microglial STING. Targeted pharmacotherapies to reduce this microglial STING response may be beneficial in reducing neuroinflammation and corresponding neurocognitive complications following TBI.

Acknowledgements

This research was supported by a National Institute of Neurological Disorders and Stroke (NINDS) R01 grant (NS118037 to JPG). JMP, ACD, and LMW are in the Neuroscience Graduate Program (NGP) at OSU. JMP and ACD were supported by OSU Distinguished University Fellowships. LMW was supported by an NINDS T32 grant (NS105864). In addition, this work was supported by an NINDS P30 Core Grant (NS045758) to the Center for Brain and Spinal Cord Repair. BioRender was used to construct Fig. 8C. The authors thank Dr. Kim Green (University of California-Irvine) and his laboratory for their help with the protocol and initial pilot study for the analyses of neurofilament light chain (NF-L) in the plasma. The authors also thank Ryan Bullard, Braedan Oliver, Zoë Tapp-Poole, and Lauren Otto (The Ohio State University) for with their technical assistance on aspects on the project.

Author contributions

All authors contributed to the study's conception and design. Material preparation and data collection were performed by JMP, SGG, LMW, ACD, and CEB. Experimental design and data analyses were performed by JMP and JPG. The manuscript was written by JMP and JPG and all authors were involved in editing. Funding acquisition, administration, and supervision were performed by JPG. All authors read and approved the final manuscript.

Funding

This research was supported by a National Institute of Neurological Disorders and Stroke (NINDS) R01 grant (NS118037 to JPG). JMP and ACD were supported by OSU Distinguished University Fellowships. LMW was supported by an NINDS T32 grant (NS105864). In addition, this work was supported by an NINDS P30 Core Grant (NS045758) to the Center for Brain and Spinal Cord Repair.

Data availability

The data that support the findings of this study are available from the corresponding author upon reasonable request.

Declarations

Ethics approval and consent for participation

We affirm that this paper contains original data that have not been submitted elsewhere for publication and that all authors have read and approved the manuscript. All authors also report no financial conflicts of interest. All procedures were performed in accordance with the National Institute of Health Guidelines for the Care and Use of Laboratory Animals, the Public Health Service's Policy on Human Care and Use of Laboratory Animals, and the Guide for the Care and Use of Laboratory Animals and were approved by The Ohio State University Institutional Laboratory Animal Care and Use Committee.

Competing interests

The authors have no financial conflicts of interest to disclose.

Author details

¹Department of Neuroscience, The Ohio State University Wexner Medical Center, 333 W 10Th Ave, Columbus, OH, USA. ²Chronic Brain Injury Program, The Ohio State University, 175 Pomerene Hall, Columbus, OH, USA. ³231 IBMR Building, The Ohio State University, 460 Medical Center Dr., Columbus, OH 43210, USA.

Received: 4 February 2025 Accepted: 18 April 2025

Published online: 30 April 2025

References

- Faul M, Coronado V. Epidemiology of traumatic brain injury. *Handb Clin Neurol.* 2015;127:3–13.
- Kokiko-Cochran ON, Godbout JP. The Inflammatory continuum of traumatic brain injury and Alzheimer's disease. *Front Immunol.* 2018;9:672.
- Wangler LM, Godbout JP. Microglia moonlighting after traumatic brain injury: aging and interferons influence chronic microglia reactivity. *Trends Neurosci.* 2023;46(11):926–40.
- Henry RJ, Loane DJ. Targeting chronic and evolving neuroinflammation following traumatic brain injury to improve long-term outcomes: insights from microglial-depletion models. *Neural Regen Res.* 2021;16(5):976–7.
- Loane DJ, et al. Progressive neurodegeneration after experimental brain trauma: association with chronic microglial activation. *J Neuropathol Exp Neurol.* 2014;73(1):14–29.
- Ramlackhansingh AF, et al. Inflammation after trauma: microglial activation and traumatic brain injury. *Ann Neurol.* 2011;70(3):374–83.
- Coughlin JM, et al. Imaging of glial cell activation and white matter integrity in brains of active and recently retired national football league players. *JAMA Neurol.* 2017;74(1):67–74.
- Coughlin JM, et al. Neuroinflammation and brain atrophy in former NFL players: an in vivo multimodal imaging pilot study. *Neurobiol Dis.* 2015;74:58–65.
- Johnson VE, et al. Inflammation and white matter degeneration persist for years after a single traumatic brain injury. *Brain.* 2013;136(Pt 1):28–42.
- Bray CE, et al. Chronic cortical inflammation, cognitive impairment, and immune reactivity associated with diffuse brain injury are ameliorated by forced turnover of microglia. *J Neurosci.* 2022;42(20):4215–28.
- Witcher KG, et al. Traumatic brain injury causes chronic cortical inflammation and neuronal dysfunction mediated by microglia. *J Neurosci.* 2021;41(7):1597–616.
- Witcher KG, et al. Traumatic brain injury-induced neuronal damage in the somatosensory cortex causes formation of rod-shaped microglia that promote astrogliosis and persistent neuroinflammation. *Glia.* 2018;66(12):2719–36.
- Henry RJ, et al. Microglial depletion with CSF1R inhibitor during chronic phase of experimental traumatic brain injury reduces neurodegeneration and neurological deficits. *J Neurosci.* 2020;40(14):2960–74.
- Gangal H, et al. Traumatic brain injury exacerbates alcohol consumption and neuroinflammation with decline in cognition and cholinergic activity. *BioRxiv.* 2024. <https://doi.org/10.1101/2024.09.21.614247>.
- Todd BP, et al. Traumatic brain injury results in unique microglial and astrocyte transcriptomes enriched for type I interferon response. *J Neuroinflammation.* 2021;18(1):151.
- Wangler LM, et al. Amplified gliosis and interferon-associated inflammation in the aging brain following diffuse traumatic brain injury. *J Neurosci.* 2022;42(48):9082–96.
- Barrett JP, et al. Traumatic brain injury induces cGAS activation and type I interferon signaling in aged mice. *Front Immunol.* 2021;12:710608.
- Boland R, Kokiko-Cochran ON. Deplete and repeat: microglial CSF1R inhibition and traumatic brain injury. *Front Cell Neurosci.* 2024;18:1352790.
- Gao X, et al. Moderate traumatic brain injury causes acute dendritic and synaptic degeneration in the hippocampal dentate gyrus. *PLoS ONE.* 2011;6(9): e24566.
- Wakade C, et al. Delayed reduction in hippocampal postsynaptic density protein-95 expression temporally correlates with cognitive dysfunction following controlled cortical impact in mice. *J Neurosurg.* 2010;113(6):195–201.
- Rice RA, et al. Microglial repopulation resolves inflammation and promotes brain recovery after injury. *Glia.* 2017;65(6):931–44.
- Packer JM, et al. Impaired cortical neuronal homeostasis and cognition after diffuse traumatic brain injury are dependent on microglia and type I interferon responses. *Glia.* 2024;72(2):300–21.
- Ishikawa H, Ma Z, Barber GN. STING regulates intracellular DNA-mediated, type I interferon-dependent innate immunity. *Nature.* 2009;461(7265):788–92.
- Decout A, et al. The cGAS-STING pathway as a therapeutic target in inflammatory diseases. *Nat Rev Immunol.* 2021;21(9):548–69.
- Abe T, Barber GN. Cytosolic-DNA-mediated, STING-dependent proinflammatory gene induction necessitates canonical NF-kappaB activation through TBK1. *J Virol.* 2014;88(10):5328–41.
- Yum S, et al. TBK1 recruitment to STING activates both IRF3 and NF-kappaB that mediate immune defense against tumors and viral infections. *Proc Natl Acad Sci USA.* 2021;118(14):e2100225118.
- Fritsch LE, et al. STING-dependent signaling in microglia or peripheral immune cells orchestrates the early inflammatory response and influences brain injury outcome. *J Neurosci.* 2024;44(12):e0191232024.
- Fritsch LE, et al. Type I interferon response is mediated by NLRX1-cGAS-STING signaling in brain injury. *Front Mol Neurosci.* 2022;15: 852243.
- Witcher KG, et al. Comparison between midline and lateral fluid percussion injury in mice reveals prolonged but divergent cortical neuroinflammation. *Brain Res.* 2020;1746: 146987.
- Bedolla AM, et al. A comparative evaluation of the strengths and potential caveats of the microglial inducible CreER mouse models. *Cell Rep.* 2024;43(1): 113660.
- Goldmann T, et al. Origin, fate and dynamics of macrophages at central nervous system interfaces. *Nat Immunol.* 2016;17(7):797–805.
- Christopher N, et al. Microglia promote learning-dependent synapse formation through brain-derived neurotrophic factor. *Cell.* 2013;155(7):1596–609.
- Yona S, et al. Fate mapping reveals origins and dynamics of monocytes and tissue macrophages under homeostasis. *Immunity.* 2013;38(1):79–91.
- Li X, et al. The effects of tamoxifen on mouse behavior. *Genes Brain Behav.* 2020;19(4):e12620.
- Fenn AM, et al. Immune activation promotes depression 1 month after diffuse brain injury: a role for primed microglia. *Biol Psychiatry.* 2014;76(7):575–84.
- O'Neil SM, et al. Forced turnover of aged microglia induces an intermediate phenotype but does not rebalance CNS environmental cues driving priming to immune challenge. *Acta Neuropathol Commun.* 2018;6(1):129.
- Tapp ZM, et al. Sleep fragmentation engages stress-responsive circuitry, enhances inflammation and compromises hippocampal function following traumatic brain injury. *Exp Neurol.* 2022;353: 114058.
- Wohleb ES, et al. Peripheral innate immune challenge exaggerated microglia activation, increased the number of inflammatory CNS macrophages, and prolonged social withdrawal in socially defeated mice. *Psychoneuroendocrinology.* 2012;37(9):1491–505.
- Muccigrosso MM, et al. Cognitive deficits develop 1 month after diffuse brain injury and are exaggerated by microglia-associated reactivity to peripheral immune challenge. *Brain Behav Immun.* 2016;54:95–109.
- Tran KM, et al. A Trem 2(R47H) mouse model without cryptic splicing drives age- and disease-dependent tissue damage and synaptic loss in response to plaques. *Mol Neurodegener.* 2023;18(1):12.
- Paolicelli RC, et al. Microglia states and nomenclature: a field at its crossroads. *Neuron.* 2022;110(21):3458–83.
- Ziebell JM, et al. Rod microglia: elongation, alignment, and coupling to form trains across the somatosensory cortex after experimental diffuse brain injury. *J Neuroinflammation.* 2012;9:247.
- Love MI, Huber W, Anders S. Moderated estimation of fold change and dispersion for RNA-seq data with DESeq2. *Genome Biol.* 2014;15(12):550.
- Kosugi M, et al. Mutations of histone demethylase genes encoded by X and Y chromosomes, Kdm5c and Kdm5d, lead to noncompaction cardiomyopathy in mice. *Biochem Biophys Res Commun.* 2020;525:100–6.
- Munoz-Ballester C, et al. Mild traumatic brain injury-induced disruption of the blood-brain barrier triggers an atypical neuronal response. *Front Cell Neurosci.* 2022;16: 821885.

46. Ritzel RM, et al. Brain injury accelerates the onset of a reversible age-related microglial phenotype associated with inflammatory neurodegeneration. *Sci Adv*. 2023;9(10):eadd1101.
47. O'Neil SM, et al. Astrocyte immunosenescence and deficits in interleukin 10 signaling in the aged brain disrupt the regulation of microglia following innate immune activation. *Glia*. 2022;70(5):913–34.
48. Graham NSN, et al. Axonal marker neurofilament light predicts long-term outcomes and progressive neurodegeneration after traumatic brain injury. *Sci Transl Med*. 2021;13(613):eabg922.
49. Sadler AJ, Williams BR. Interferon-inducible antiviral effectors. *Nat Rev Immunol*. 2008;8(7):559–68.
50. Barrett JP, et al. Interferon-beta plays a detrimental role in experimental traumatic brain injury by enhancing neuroinflammation that drives chronic neurodegeneration. *J Neurosci*. 2020;40(11):2357–70.
51. Todd BP, et al. Selective neuroimmune modulation by type I interferon drives neuropathology and neurologic dysfunction following traumatic brain injury. *Acta Neuropathol Commun*. 2023;11(1):134.
52. Goodman EJ, et al. Enhanced fear memory after social defeat in mice is dependent on interleukin-1 receptor signaling in glutamatergic neurons. *Mol Psychiatry*. 2024;29:2321–34.
53. Goodman EJ, et al. Novel microglial transcriptional signatures promote social and cognitive deficits following repeated social defeat. *Commun Biol*. 2024;7(1):1199.
54. Loda A, Heard E. Xist RNA in action: past, present, and future. *PLoS Genet*. 2019;15(9): e1008333.
55. Xu J, et al. Sex-specific differences in expression of histone demethylases Utx and Uty in mouse brain and neurons. *J Neurosci*. 2008;28(17):4521–7.
56. Shen H, et al. Sexually dimorphic RNA helicases DDX3X and DDX3Y differentially regulate RNA metabolism through phase separation. *Mol Cell*. 2022;82(14):2588–2603 e9.
57. Abdullah A, et al. STING-mediated type-I interferons contribute to the neuroinflammatory process and detrimental effects following traumatic brain injury. *J Neuroinflammation*. 2018;15(1):323.
58. Sen T, et al. Aberrant ER stress induced neuronal-IFNbeta elicits white matter injury due to microglial activation and T-cell infiltration after TBI. *J Neurosci*. 2020;40(2):424–46.
59. Bachstetter AD, et al. Rod-shaped microglia morphology is associated with aging in 2 human autopsy series. *Neurobiol Aging*. 2017;52:98–105.
60. Xie M, et al. Rod-shaped microglia interact with neuronal dendrites to regulate cortical excitability in TDP-43 related neurodegeneration. *BioRxiv*. 2024. <https://doi.org/10.1101/2024.06.30.601396>.
61. Wang Y, et al. Inflammasome activation triggers caspase-1-mediated cleavage of cGAS to regulate responses to DNA virus infection. *Immunity*. 2017;46(3):393–404.
62. Liu X, et al. Interleukin 1 type 1 receptor restore: a genetic mouse model for studying interleukin 1 receptor-mediated effects in specific cell types. *J Neurosci*. 2015;35(7):2860–70.
63. Vincent JC, et al. IL-1R1 signaling in TBI: assessing chronic impacts and neuroinflammatory dynamics in a mouse model of mild closed-head injury. *J Neuroinflammation*. 2023;20(1):248.
64. Escoubas CC, et al. Type-I-interferon-responsive microglia shape cortical development and behavior. *Cell*. 2024;187(8):1936–1954 e24.
65. Hosseini S, et al. Type I interferon receptor signaling in astrocytes regulates hippocampal synaptic plasticity and cognitive function of the healthy CNS. *Cell Rep*. 2020;31(7): 107666.
66. Hashemzadeh-Bonehi L, et al. Pin1 protein associates with neuronal lipofuscin: potential consequences in age-related neurodegeneration. *Exp Neurol*. 2006;199(2):328–38.
67. Richter S, et al. Prognostic value of serum biomarkers in patients with moderate-severe traumatic brain injury, differentiated by marshall computer tomography classification. *J Neurotrauma*. 2023;40(21–22):2297–310.
68. Scott G, et al. Minocycline reduces chronic microglial activation after brain trauma but increases neurodegeneration. *Brain*. 2018;141(2):459–71.
69. Brennan FH, et al. Microglia coordinate cellular interactions during spinal cord repair in mice. *Nat Commun*. 2022;13(1):4096.
70. Tariq K, et al. Disruption of mTORC1 rescues neuronal overgrowth and synapse function dysregulated by Pten loss. *Cell Rep*. 2022;41(5): 111574.
71. Liu R, et al. BpV(pic) confers neuroprotection by inhibiting M1 microglial polarization and MCP-1 expression in rat traumatic brain injury. *Mol Immunol*. 2019;112:30–9.
72. Metcalfe M, Steward O. PTEN deletion in spinal pathways via retrograde transduction with AAV-RG enhances forelimb motor recovery after cervical spinal cord injury; sex differences and late-onset pathophysiology. *Exp Neurol*. 2023;370: 114551.
73. Doran SJ, et al. Sex differences in acute neuroinflammation after experimental traumatic brain injury are mediated by infiltrating myeloid cells. *J Neurotrauma*. 2019;36(7):1040–53.
74. Villapol S, Loane DJ, Burns MP. Sexual dimorphism in the inflammatory response to traumatic brain injury. *Glia*. 2017;65(9):1423–38.
75. Starkey NJ, et al. Sex differences in outcomes from mild traumatic brain injury eight years post-injury. *PLoS ONE*. 2022;17(5): e0269101.
76. Iannucci J, et al. Sex-specific and traumatic brain injury effects on dopamine receptor expression in the hippocampus. *Int J Mol Sci*. 2023;24(22):16084.
77. Corona AW, et al. Fractalkine receptor (CX3CR1) deficiency sensitizes mice to the behavioral changes induced by lipopolysaccharide. *J Neuroinflammation*. 2010;7:93.
78. Febinger HY, et al. Time-dependent effects of CX3CR1 in a mouse model of mild traumatic brain injury. *J Neuroinflammation*. 2015;12:154.
79. Wang W, et al. CX3CR1 deficiency aggravates brain white matter injury and affects expression of the CD36/15LO/NR4A1 signal. *Biochem Biophys Res Commun*. 2021;549:47–53.

Publisher's Note

Springer Nature remains neutral with regard to jurisdictional claims in published maps and institutional affiliations.